

Provided for non-commercial research and education use.  
Not for reproduction, distribution or commercial use.



This article was published in an Elsevier journal. The attached copy is furnished to the author for non-commercial research and education use, including for instruction at the author's institution, sharing with colleagues and providing to institution administration.

Other uses, including reproduction and distribution, or selling or licensing copies, or posting to personal, institutional or third party websites are prohibited.

In most cases authors are permitted to post their version of the article (e.g. in Word or Tex form) to their personal website or institutional repository. Authors requiring further information regarding Elsevier's archiving and manuscript policies are encouraged to visit:

<http://www.elsevier.com/copyright>



# A computational model of adipose tissue metabolism: Evidence for intracellular compartmentation and differential activation of lipases

Jaeyeon Kim<sup>a,b</sup>, Gerald M. Saidel<sup>a,b</sup>, Satish C. Kalhan<sup>b,c,\*</sup>

<sup>a</sup>Department of Biomedical Engineering, Case Western Reserve University, Cleveland, OH 44106, USA

<sup>b</sup>Center for Modeling Integrated Metabolic Systems, Case Western Reserve University, Cleveland, OH 44106, USA

<sup>c</sup>Department of Medicine, Cleveland Clinic Lerner College of Medicine, Case Western Reserve University, Cleveland, OH 44106, USA

Received 26 September 2007; received in revised form 30 November 2007; accepted 11 December 2007

Available online 15 December 2007

## Abstract

Regulation of lipolysis in adipose tissue is critical to whole body fuel homeostasis and to the development of insulin resistance. Due to the challenging nature of laboratory investigations of regulatory mechanisms in adipose tissue, mathematical models could provide a valuable adjunct to such experimental work. We have developed a computational model to analyze key components of adipose tissue metabolism *in vivo* in human in the fasting state. The various key components included triglyceride-fatty acid cycling, regulation of lipolytic reactions, and glyceroneogenesis. The model, consisting of spatially lumped blood and cellular compartments, included essential transport processes and biochemical reactions. Concentration dynamics for major substrates were described by mass balance equations. Model equations were solved numerically to simulate dynamic responses to intravenous epinephrine infusion. Model simulations were compared with the corresponding experimental measurements of the arteriovenous difference across the abdominal subcutaneous fat bed in humans. The model can simulate physiological responses arising from the different expression levels of lipases. Key findings of this study are as follows: (1) Distinguishing the active metabolic subdomain (~3% of total tissue volume) is critical for simulating data. (2) During epinephrine infusion, lipases are differentially activated such that diglyceride breakdown is approximately four times faster than triglyceride breakdown. (3) Glyceroneogenesis contributes more to glycerol-3-phosphate synthesis during epinephrine infusion when pyruvate oxidation is inhibited by a high acetyl-CoA/free-CoA ratio.

© 2008 Elsevier Ltd. All rights reserved.

**Keywords:** Epinephrine; Lipolysis; Mathematical model

## 1. Introduction

Adipose tissue is no longer considered a metabolically quiescent storage depot of lipids, but an active organ that regulates plasma fatty acid (FA) levels (Frayn, 2002; Frayn et al., 2003) and secretes various cytokines and hormones such as leptin, adiponectin, resistin, tumor necrosis factor (TNF)- $\alpha$ , etc. (Trayhurn and Beattie, 2001; Frayn et al., 2003). The understanding of adipose tissue metabolism and its regulation is underscored by the demonstration of its

role in the development of insulin resistance, regulation of satiety, and other metabolic functions (Kahn et al., 2006; Frayn, 2001).

Since adipose tissue does not have a unique artery (inflow) and vein (outflow), reliable *in vivo* data across this tissue are limited. In fact, the only location available for arteriovenous difference (AVD) measurement in human is the subcutaneous fat bed in the abdominal wall (Samra et al., 1996; Frayn et al., 1994; Coppack et al., 1990). Based on data from this single depot, generalizations cannot be made about all metabolically heterogeneous depots (subcutaneous vs. visceral) of adipose tissue (Jensen, 2002). As an alternative, *in vivo* microdialysis has been applied to study adipose tissue metabolism in human, but it provides only qualitative data of several metabolites in the interstitium. *In vitro* studies of tissue explants or isolated cells

\*Corresponding author at: Department of Pathobiology, Lerner Research Institute, NE4-203, Cleveland Clinic Foundation, 9500 Euclid Avenue, Cleveland, OH 44195, USA. Tel.: +1 216 444 3445; fax: 1 216 636 1493.

E-mail address: [satish.kalhan@case.edu](mailto:satish.kalhan@case.edu) (S.C. Kalhan).

do not provide comparable physiological data with respect to *in vivo* conditions (Frayn et al., 2003). Mathematical models and simulations of adipose tissue metabolism *in vivo* offer a method for quantitative analysis of control mechanisms for lipid mobilization and for prediction of physiological responses.

Adipose tissue comprises about 20% of body weight but its rate of utilizing oxygen in the basal state is less than 2% of whole body rate of oxygen consumption (Frayn et al., 1995). Despite its negligible contribution to energetics, it actively participates in the whole body fuel homeostasis by modulating lipid metabolism. Regulation of breakdown (lipolysis) and synthesis (esterification) of triglycerides (TG) in adipose tissue controls lipid flux into circulation. Since adipose tissue via lipolysis releases more FA into circulation than required for oxidation, a significant part of the released FA are re-esterified in adipose tissue and in other organs. This triglyceride–fatty acid (TG–FA) cycle, is composed of an intra-adipose tissue cycle and an extra-adipose tissue cycle. FA released into plasma are taken up by the liver, re-esterified, and secreted as very large density lipoprotein (VLDL)-TG, which are then transported to the periphery to be reincorporated into adipose tissue TG (Newsholme and Crabtree, 1976; Klein and Wolfe, 1990; Frayn et al., 1994). As proposed by Newsholme and Crabtree (1976), the existence of TG–FA cycle provides for increased sensitivity and flexibility in controlling lipid mobilization.

Hormone-sensitive lipase (HSL) was considered the only rate-limiting enzyme for lipolysis of TG in adipose tissue (Large et al., 1998). However, recently, it has been shown that the HSL-deficient mice retain the basal lipolysis rate and respond to the beta-adrenergic stimulation, although the response was quantitatively less than in the wild type (Okazaki et al., 2002; Zechner et al., 2005; Haemmerle et al., 2002). The accumulation of diglycerides (DG) in the adipose tissue of HSL knockout mice suggests that HSL is the rate-limiting enzyme for the hydrolysis of DG and not TG (Haemmerle et al., 2002). Adipose TG lipase (ATGL) has been suggested to be the key enzyme involved in TG hydrolysis in the adipose tissue (Schweiger et al., 2006; Haemmerle et al., 2006; Zimmermann et al., 2004). TG lipolysis was shown to be severely impaired in ATGL-deficient mice, accumulating large amount of fat in major organs and leading to premature death (Haemmerle et al., 2006). The integrated response of these lipase reactions is essential to understand the metabolic regulation of lipolysis in the adipose tissue.

Re-esterification of fatty acids requires a source of glycerol-3-phosphate (G3P). Since the activity of glycerol kinase is very low in the adipose tissue (Edens et al., 1990b), it cannot form G3P from glycerol in significant quantities. Instead, glucose and/or pyruvate are utilized to produce G3P. The use of pyruvate to form G3P has been termed glyceroneogenesis (Reshef et al., 2003). Quantitative estimation of glyceroneogenesis has not been performed in human *in vivo*. Animal studies using isotopic

tracers have shown that glyceroneogenesis is the dominant pathway in different physiological and nutritional conditions (Tordjman et al., 2003; Brito et al., 2006; C.K. Nye, R.W. Hanson, and S.C. Kalhan, unpublished data). These data underscore the need to examine the metabolism of the precursors for G3P by the adipose tissue.

In the present study, we have developed a mathematical model of adipose tissue metabolism *in vivo* in human in the fasting state and investigated the integrated response to increased lipolysis induced by epinephrine. The intravenous epinephrine infusion study in human inguinal fat bed was used to validate the model simulations (Samra et al., 1996). We assessed the capability of the model to reproduce and predict the physiological responses to enzymatic modulation in steady state by altering the expression levels of ATGL and HSL. We hypothesized that a metabolic subdomain exists in the adipose tissue due to the large volume fraction of lipid droplets and most of metabolic reactions occur in a small region of adipose tissue. In addition, we postulated that the individual lipase reactions are differentially activated during epinephrine infusion resulting in the distinctive dynamics of lipolytic intermediates (i.e., DG, MG). Finally, we used this model to predict the source of G3P. We hypothesized that the increase in FA levels during epinephrine infusion inhibits pyruvate oxidation and increases glyceroneogenesis.

## 2. Methods

A mathematical model of adipose tissue metabolism was developed that incorporates essential transport and reaction processes. The model is composed of spatially lumped cellular and blood compartments. Exchange of substrates occurs between the two compartments via simple diffusion or carrier-mediated transport. For a minimal representation of the consequences of glucose and fatty acid metabolism, individual metabolic pathways are lumped to include at least one irreversible reaction step favoring the formation of product (Fig. 1). The reversible reactions catalyzed by lactate dehydrogenase (LDH) and G3P dehydrogenase have forward and reverse rate coefficients that are related by the thermodynamic constraint (Supplementary Material). Pathways associated with TG breakdown and synthesis include various lipolytic intermediates (i.e., DG, MG) and regulatory enzymes, i.e., ATGL, HSL, MGL (monoglyceride lipase) as shown in Fig. 1.

### 2.1. Chemical species

The major metabolic species related to glucose and fatty acid metabolism were incorporated into the model. Glycolytic species included glucose (GLC), glucose-6-phosphate (G6P), glycerol-3-phosphate (G3P), glyceraldehydes-3-phosphate (GAP), pyruvate (PYR), and lactate (LAC). Chemical species for lipid metabolism included FA, TG, DG, MG, fatty acyl-CoA (FAC), free CoA, and

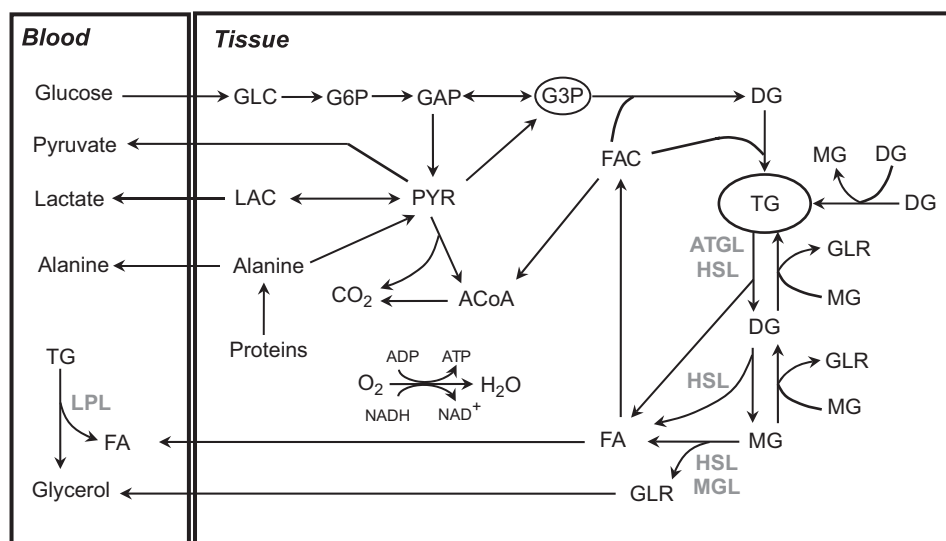


Fig. 1. Metabolic pathways involved in triglycerides synthesis and breakdown in the adipose tissue. As shown, glucose is taken up from, and pyruvate, lactate, free fatty acids, glycerol, and alanine are released, into the blood compartment. Alanine is considered to represent all amino acids released by protein breakdown. Glycerol-3-phosphate, used for the esterification of fatty acids, is formed either from glucose via glycolysis or from pyruvate via glyceroneogenesis. The various steps in the esterification and hydrolysis of triglycerides are shown. ATP–ADP and/or NADH–NAD<sup>+</sup> are used as co-substrates in the model, but are not shown except for the oxidative phosphorylation. The arrow with both ends indicates a reversible reaction step. GLC, glucose; PYR, pyruvate; LAC, lactate; ALA, alanine; GLR, glycerol; FA, fatty acids; G6P, glucose-6-phosphate; GAP, glyceraldehyde-3-phosphate; G3P, glycerol-3-phosphate; ACoA, acetyl CoA; FAC, fatty acyl CoA; TG, triglycerides; DG, diglycerides; MG, monoglycerides; LPL, lipoprotein lipase; ATGL, adipose triglyceride lipase; HSL, hormone-sensitive lipase; MGL, monoglyceride lipase.

glycerol (GLR). Palmitate with 16 carbons was considered to represent all FAs. TG, DG, and MG were considered esterified products of G3P and palmitate. Acetyl-CoA (ACoA) and oxygen were included for substrate oxidation. ATP, ADP, inorganic phosphate (Pi), NADH, and NAD<sup>+</sup> were incorporated into the reaction steps where they were required as co-substrates. Finally, alanine (ALA) was used as the representative amino acid.

## 2.2. Model specifications and assumptions

The basal condition for model simulations was the overnight fasted human at rest. Data from arteriovenous balance studies of the subcutaneous adipose tissue bed (Frayn et al., 1991, 1994, 1995; Coppack et al., 1990) and biochemical data of enzyme activity (Zechner et al., 2005; Shen et al., 1998; Large et al., 1998), were utilized to develop the framework of metabolic fluxes. Various assumptions were required in the absence of experimental data.

### 2.2.1. Carbohydrate and energy metabolism

Glucose and FA are the major fuels for adipose tissue. Approximately 50% of the glucose taken up by the adipose tissue is used for oxidative metabolism and about 40% is released as lactate (Frayn et al., 1995; Coppack et al., 1990). FA oxidation accounted for the remaining oxygen consumption. The relative contribution of glucose and FA to oxidative metabolism is consistent with reported respiratory quotient (RQ) of 0.91 (Coppack et al., 1990). Synthesis and breakdown of glycogen were considered to

be negligible (Jurczak et al., 2007). We assumed that less than 10% of glucose uptake was converted to G3P, which can also be formed from pyruvate via glyceroneogenesis (Reshef et al., 2003). Uptake of glucose and release of lactate by the adipose tissue of humans indicates a significant glycolytic contribution to G3P (Coppack et al., 1990). In contrast, animal studies using isotopic tracers have shown glyceroneogenesis to be the major pathway for G3P synthesis under different physiological and nutritional conditions (Tordjman et al., 2003; Brito et al., 2006). Therefore, we assumed equal contribution of glycolysis and glyceroneogenesis in the basal state. However, we investigated the effects of different weightings of the two pathways during epinephrine infusion.

### 2.2.2. Lipid metabolism

The contribution of lipolysis in the blood compartment by lipoprotein lipase (LPL) was determined from the AVD of TG in adipose tissue bed (Samra et al., 1996). The intracellular rates of lipolysis by ATGL, HSL, and MGL were estimated from the difference between AVDs of glycerol and TG such that ~15% of the produced FA are re-utilized inside adipose tissue (Frayn et al., 1994; Coppack et al., 1990). Finally, fluxes through individual lipase reaction were estimated based on the 10-fold higher activity that HSL has for DG than for TG and MG (Shen et al., 1998; Haemmerle et al., 2002). Thus, the flux rate for DG breakdown by HSL was calculated first and then those for TG and MG breakdown by HSL. The maximum rate coefficient of HSL ( $V_{max,k}$ ) for TG and MG breakdown were 10-times lower than that for DG breakdown.

Although FA can be transported by both simple diffusion and carrier-mediated transport (Bradbury, 2006), the simple diffusion of FA was assumed in this model.

### 2.2.3. Amino acid metabolism

A net release of amino acids into plasma from adipose tissue occurs in the fasting state (Patterson et al., 2002). Alanine and glutamine are released in significant quantities and there is a net uptake of glutamate by the adipose tissue (Fraysn et al., 1991). The net release of amino acids by the adipose tissue and the rate of proteolysis in the adipose tissue were used to calculate the mass transport and the rates of appearance of amino acids as represented by alanine (Patterson et al., 2002; Coppack et al., 1996).

### 2.2.4. Reaction kinetics

Kinetic expressions based on *in vitro* data for each elementary enzymatic reaction were not feasible for this *in vivo* study. Instead, we used a phenomenological Michaelis–Menten (M–M) equation constrained by the physiological conditions. We assumed that all metabolic reactions are expressed by a general bi–bi M–M form. The kinetic parameters such as the phenomenological M–M constants (i.e.,  $K_{m,k}$ ,  $K_{i,k}$ ,  $K_{f,k}$  and  $K_{b,k}$ ) were set to the initial tissue concentrations of the corresponding substrates. Since we used a top-down approach to relate the responses of different scales (i.e., cellular and tissue levels), several reaction steps are lumped. Palmitate and alanine represent the entire family of fatty acids and amino acids. The efficacy of this approach has been demonstrated in other studies (Kim et al., 2007; Zhou et al., 2005). Since the maximum rate coefficients are determined from *in vivo* flux data and the phenomenological M–M constants, the metabolic fluxes described by this method can be bounded within physiological limits.

### 2.2.5. Intracellular compartmentation

Due to the large volume fraction of lipid droplets in adipocyte, we postulated that the most of metabolites are localized in a small sub-cellular domain. The effect of cellular localization of chemical species was examined by modulating the volume fraction of adipose cellular compartment ( $v_{cf}$ ). The cellular volume fraction assuming localization was optimally estimated using data from the literature. For comparison, simulation without localization assumed the physical volume fraction of adipose tissue cells ( $v_{cf} = 0.8$ ). TG, DG, and MG, whose concentrations are high compared with other substrates, were not assumed localized in the subdomain.

### 2.2.6. Activation of lipolytic reactions

HSL can breakdown all lipolytic intermediates (i.e., TG, DG and MG), while ATGL is responsible for hydrolyzing TG only (Large et al., 2004; Langin and Arner, 2006; Zechner et al., 2005). The breakdown of MG is not subject to the beta-adrenergic stimulation (Large et al., 2004;

Zechner et al., 2005). We assumed that the following three lipolytic reactions are subject to the beta-adrenergic stimulation: (1) TG breakdown to DG by ATGL, (2) TG breakdown to DG by HSL, and (3) DG breakdown to MG by HSL. We compared two different schemes for activating lipolytic reactions. We tested the hypothesis that individual lipolytic reactions were differentially activated during epinephrine infusion as quantified by different degree of activation ( $\lambda_k$ ). Thus, the rates of TG and DG breakdowns could be increased to different extents. Simulations of differential activation for lipase reactions were compared with simulations of uniform activation ( $\lambda_k$ ) values so that TG and DG breakdowns have the same stimulation.

### 2.2.7. Beta-adrenergic stimulation

Cyclic-AMP (cAMP) dependent protein kinase A (PKA) phosphorylates HSL and other proteins including perilipin upon beta-adrenergic stimulation (Brasaemle et al., 2000). The time scale of increase in cAMP levels and activation of PKA is reported to be less than 1 min (Honnor et al., 1985). In contrast, the response to the intravenous epinephrine infusion showed that the peak concentration of venous epinephrine was reached after  $\sim 30$  min (Samra et al., 1996). The time scales of fatty acids and glycerol releases were more comparable to that of venous epinephrine levels (Samra et al., 1996). Consequently, the effect of instantaneous changes in cAMP levels on the simulated responses would be negligible in the time frame of our model simulation ( $\sim 60$  min). Therefore, we have lumped all the cascade controls of the molecular level regulatory mechanisms into the action of epinephrine by introducing a phenomenological equation relating the activation of lipolytic reactions to the venous epinephrine levels. With this algorithm, the modulation of maximum rate constants ( $V_{max}$ ) by epinephrine represents not only the activation of lipase, but also concomitant activation of other proteins including perilipin.

## 2.3. Dynamic mass balance equations

The dynamic mass balance equations describe changes in substrate concentration in blood and adipose cells in tissue. The blood compartment represents plasma in equilibrium with interstitial fluid. The concentration of substrate  $i$  in the blood compartment is determined by

$$V_b \frac{dC_{b,i}}{dt} = Q(C_{a,i} - C_{b,i}) + R_{b,i} - J_{b \leftrightarrow c,i}, \quad (1)$$

where  $C_{a,i}$  is the arterial concentration;  $C_{b,i}$  is the capillary blood concentration (equal to the adipose venous concentration  $C_{v,i}$ );  $Q$  is the blood flow in adipose tissue;  $J_{b \leftrightarrow c,i}$  is the net mass transport flux across the blood–cell exchange barrier;  $R_{b,i}$  is the net metabolic reaction rate of substrate  $i$  in the blood compartment;  $V_b$  is the volume of blood compartment, which is equal to the physical volume of capillary blood and interstitial fluid comprising 20% of total tissue volume ( $V_{tissue}$ ). Since oxygen and carbon

dioxide are transported as free and bound forms in the blood, the effective volume of the blood compartment is different from the physical volume as shown in Supplementary Material.

In the adipose cellular compartment, the dynamic mass equation of substrate  $i$  is

$$V_c \frac{dC_{c,i}}{dt} = R_{c,i} + J_{b \leftrightarrow c}, \quad (2)$$

where  $C_{c,i}$  is the cellular concentration;  $R_{c,i}$  is the net metabolic reaction rate of substrate  $i$ ; and  $V_c$  is the volume of the cellular compartment.

For convenience in simulation, the compartment volumes in Eqs. (1) and (2) were replaced with the volume fractions ( $v_{bf} = V_b/V_{tissue}$  or  $v_{cf} = V_c/V_{tissue}$ ). Consequently, blood flow and rate coefficients in this model are specified per unit volume of tissue. For comparison to experimental data, the blood flow, AVD, and metabolic reaction rates from the model equations were converted from a tissue volume basis to a tissue wet weight basis by division with mass density.

#### 2.4. Mass transport flux between blood and tissue

The substrates involved in blood–tissue transport are glucose, lactate, pyruvate, alanine, glycerol, FA, carbon dioxide, and oxygen. They are transported via either simple diffusion or carrier-mediated (facilitated) transport. The mass transport flux of glycerol, FA, oxygen and carbon dioxide between blood and cell ( $J_{b \leftrightarrow c,i}$ ) occurs by passive diffusion:

$$J_{b \leftrightarrow c,i} = \gamma_i (C_{b,i} - C_{c,i}), \quad (3a)$$

where  $\gamma_i$  is the mass transport coefficient of substrate  $i$ . The mass transport flux of glucose, pyruvate, lactate and alanine occurs by facilitated transport:

$$J_{b \leftrightarrow c,i} = T_{max,i} \left( \frac{C_{b,i}}{M_{m,i} + C_{b,i}} - \frac{C_{c,i}}{M_{m,i} + C_{c,i}} \right), \quad (3b)$$

where  $T_{max,i}$  is the maximum mass transport coefficient of substrate  $i$  and  $M_{m,i}$  is the M–M constant of substrate  $i$ .

#### 2.5. Metabolic flux

The metabolic reaction rates ( $R_{x,i}$ ,  $x = b$  or  $c$ ) are the net result of metabolic reactions producing and utilizing the corresponding substrate:

$$R_{x,i} = \sum_k \alpha_{i,k} \phi_{x,k}, \quad x = b \text{ or } c, \quad (4)$$

where  $\phi_{x,k}$  is the flux rate of the metabolic reaction  $k$  including substrate  $i$ ;  $\alpha_{i,k}$  is the corresponding stoichiometric coefficient, which is either positive (product) or negative (reactant). The net reaction rate for each substrate is shown in Table 1.

Metabolic fluxes are expressed with a general irreversible  $bi$ – $bi$  substrate to product enzymatic reaction coupled with

controller energy metabolite pairs (Kim et al., 2007).



where  $E_1$  and  $E_2$  are ATP and ADP or vice-versa, and/or NADH and  $NAD^+$  or vice-versa. The corresponding reaction flux equation for flux  $k$  can be expressed as:

$$\phi_k = V_{max,k} \left( \frac{PS^\pm}{\mu^\pm + PS^\pm} \right) \left( \frac{RS^\pm}{v^\pm + RS^\pm} \right) \times \left( \frac{C_X C_Y}{K_{m,k} + C_V C_W K_{m,k} / K_{i,k} + C_X C_Y} \right), \quad (5)$$

where  $C_X$ ,  $C_Y$ ,  $C_V$ , and  $C_W$  are reactant and product concentrations;  $V_{max,k}$  is the maximum rate coefficient in flux  $k$ ;  $K_{m,k}$  is the phenomenological M–M constant for the reactants;  $K_{i,k}$  is the constant for the product inhibition. Product inhibition occurs only in reactions specified in Supplementary Material.  $PS^+$  ( $= C_{ATP}/C_{ADP}$ ) and  $RS^+$  ( $= C_{NADH}/C_{NAD^+}$ ) indicate cellular phosphorylation and redox states. For some reactions, the effect of these controllers can be in the opposite direction. In this case,  $PS^- = 1/PS^+$  and  $RS^- = 1/RS^+$ . In addition,  $\mu^\pm$  and  $v^\pm$  are parameters for the metabolic controllers.

Fluxes of lactate dehydrogenase and G3P dehydrogenase reactions, which can be close to thermodynamic equilibrium, are described as reversible reactions:

$$\phi_k = \frac{V_{f,k}(C_X C_Y / K_{f,k}) - V_{b,k}(C_V C_W / K_{b,k})}{1 + (C_X C_Y / K_{f,k}) + (C_V C_W / K_{b,k})}, \quad (6)$$

where  $V_{f,k}$  and  $V_{b,k}$  are the forward and reverse rate coefficients;  $K_{f,k}$  and  $K_{b,k}$  are the phenomenological M–M constants for reactants and products;  $K_{eq}$  is the equilibrium constant calculated from the Gibbs free energy of reaction. The reaction rate coefficients are related by a thermodynamic constraint (or Haldane relationship):

$$V_{f,k} = V_{b,k} \frac{K_{eq} K_{f,k}}{K_{b,k}}. \quad (7)$$

In the blood compartment, the breakdown of TG to FAs and glycerol is the only reaction that is catalyzed by LPL. Since some LPL is carried by blood (Karpe et al., 1998), the activity of LPL reaction depends on adipose blood flow:

$$\phi_{TG \rightarrow GLR,LPL} = V_{max,LPL} \left( \frac{C_{b,TG}}{K_{m,LPL} + C_{b,TG}} \right) \left( \frac{Q}{K_{m,Q} + Q} \right), \quad (8)$$

where  $K_{m,LPL}$  and  $K_{m,Q}$  are phenomenological M–M constants for the LPL reaction.

In addition to the metabolic control by the cellular phosphorylation and redox state, epinephrine provides further regulation by stimulating lipolysis reactions governed by ATGL and HSL. The maximum rate coefficients for these three reactions undergo the further modulation by epinephrine according to an empirical relation

Table 1  
Net reaction rate ( $R_{b,i}$  or  $R_{c,i}$ ) for each substrate in blood and cellular compartments

Substrate	Net reaction rate, $R_{b,i}$ or $R_{c,i}$
<i>Blood</i>	
GLR	$\phi_{TG \rightarrow GLR,LPL}$
FA	$3\phi_{TG \rightarrow GLR,LPL}$
TG	$-\phi_{TG \rightarrow GLR,LPL}$
<i>Cells</i>	
GLC	$-\phi_{GLC \rightarrow G6P}$
PYR	$\phi_{GAP \rightarrow PYR} + \phi_{ALA \rightarrow PYR} - \phi_{PYR \leftrightarrow LAC} - \phi_{PYR \rightarrow G3P} - \phi_{PYR \rightarrow ACoA}$
LAC	$\phi_{PYR \leftrightarrow LAC}$
ALA	$-\phi_{ALA \rightarrow PYR} + \phi_{Proteolysis}$
GLR	$\phi_{MG \rightarrow GLR,MGL} + \phi_{MG \rightarrow GLR,HSL} + 0.5\phi_{MG-MG \rightarrow DG} + \phi_{MG-DG \rightarrow TG} - \phi_{GLR \rightarrow G3P}$
FA	$\phi_{TG \rightarrow DG,ATGL} + \phi_{TG \rightarrow DG,HSL} + \phi_{DG \rightarrow MG,HSL} + \phi_{MG \rightarrow GLR,HSL} + \phi_{MG \rightarrow GLR,MGL} - \phi_{FA \rightarrow FAC}$
TG	$\phi_{DG \rightarrow FAC} + 0.5\phi_{DG-DG \rightarrow TG} + \phi_{DG-MG \rightarrow TG} - \phi_{TG \rightarrow DG,ATGL} - \phi_{TG \rightarrow DG,HSL}$
O <sub>2</sub>	$-\phi_{O_2 \rightarrow H_2O}$
CO <sub>2</sub>	$\phi_{PYR \rightarrow ACoA} + 2\phi_{ACoA \rightarrow CO_2}$
G6P	$\phi_{GLC \rightarrow G6P} - \phi_{G6P \rightarrow GAP}$
GAP	$2\phi_{G6P \rightarrow GAP} - \phi_{GAP \rightarrow PYR} - \phi_{GAP \leftrightarrow G3P}$
G3P	$\phi_{GAP \leftrightarrow G3P} + \phi_{PYR \rightarrow G3P} + \phi_{GLR \rightarrow G3P} - \phi_{G3P-FAC \rightarrow DG}$
ACoA	$\phi_{PYR \rightarrow ACoA} + 8\phi_{FAC \rightarrow ACoA} - \phi_{ACoA \rightarrow CO_2}$
FAC	$\phi_{FA \rightarrow FAC} - 8\phi_{FAC \rightarrow ACoA} - 2\phi_{G3P \rightarrow DG} - \phi_{DG \rightarrow TG}$
CoA	$2\phi_{G3P \rightarrow DG} + \phi_{DG \rightarrow TG} + \phi_{ACoA \rightarrow CO_2} - \phi_{PYR \rightarrow ACoA} - \phi_{FA \rightarrow FAC} - 7\phi_{FAC \rightarrow ACoA}$
DG	$\phi_{TG \rightarrow DG,ATGL} + \phi_{TG \rightarrow DG,HSL} + \phi_{G3P \rightarrow DG} + 0.5\phi_{MG-MG \rightarrow DG} - \phi_{DG \rightarrow MG,HSL} - \phi_{DG \rightarrow TG} - \phi_{MG-DG \rightarrow TG} - \phi_{DG-DG \rightarrow TG}$
MG	$\phi_{DG \rightarrow MG,HSL} + 0.5\phi_{DG-DG \rightarrow TG} - \phi_{MG \rightarrow GLR,HSL} - \phi_{MG \rightarrow GLR,MGL} - \phi_{MG-DG \rightarrow TG} - \phi_{MG-MG \rightarrow DG}$
ATP	$2\phi_{GAP \rightarrow PYR} + \phi_{ACoA \rightarrow CO_2} + 6\phi_{O_2 \rightarrow H_2O} - \phi_{GLC \rightarrow G6P} - \phi_{G6P \rightarrow GAP} - 3\phi_{PYR \rightarrow G3P} - 2\phi_{FA \rightarrow FAC} - \phi_{GLR \rightarrow G3P} - \phi_{ATP \rightarrow ADP}$
ADP	$-R_{c,ATP}$
Pi	$2\phi_{PYR \rightarrow G3P} + 2\phi_{FA \rightarrow FAC} + \phi_{G3P \rightarrow DG} + \phi_{ATP \rightarrow ADP} - \phi_{GAP \rightarrow PYR} - \phi_{ACoA \rightarrow CO_2} - 6\phi_{O_2 \rightarrow H_2O}$
NAD <sup>+</sup>	$\phi_{PYR \leftrightarrow LAC} + \phi_{GAP \leftrightarrow G3P} + 2\phi_{PYR \rightarrow G3P} + 2\phi_{O_2 \rightarrow H_2O} - \phi_{GAP \rightarrow PYR} - \phi_{PYR \rightarrow ACoA} - 14\phi_{FAC \rightarrow ACoA} - 4\phi_{ACoA \rightarrow CO_2}$
NADH	$-R_{c,NAD^+}$

GLC, glucose; PYR, pyruvate; LAC, lactate; ALA, alanine; GLR, glycerol; FA, fatty acids; G6P, glucose-6-phosphate; GAP, glyceraldehyde-3-phosphate; G3P, glycerol-3-phosphate; ACoA, acetyl CoA; FAC, fatty acyl CoA; CoA, free CoA; Pi, inorganic phosphate.  $\phi_{A \rightarrow B}$  is the flux rate of the metabolic reaction.

(Kim et al., 2007):

$$V_{max,k} = V_{max,k}^0 \left( 1.0 + \lambda_k \frac{(C_E(t) - C_E(0))^2}{\alpha + (C_E(t) - C_E(0))^2} \right), \quad (9)$$

where  $C_E(t)$  is the epinephrine concentration in adipose venous at time  $t$ ;  $V_{max,k}^0$  is the basal state maximum rate coefficient;  $\lambda_k$  and  $\alpha$  are parameters. Here,  $\lambda_k$  indicates the degree of activation for a corresponding lipolytic reaction.

## 2.6. Parameter determination at basal state

Starting with the mass transport fluxes (Table 2), the unknown flux rates were determined with appropriate assumptions on fuel metabolism as described above. Once all the metabolic fluxes were estimated (Tables 3 and 4), then parameter values at basal state were determined together with the metabolite concentrations in blood and tissue (Tables 5 and 6). Since 60–85% of adipose tissue is lipids with 90–99% being TG (Albright and Stern, 1998), the concentrations of non-lipid substrates in total tissue

Table 2  
Basal mass transfer flux rates between blood and cells, and associated parameters

Substrate	$J_{b \leftrightarrow c,i}$ <sup>a</sup>	$T_{max,i}$ <sup>b</sup>	$M_{m,i}$ <sup>c</sup>	$\gamma_i$ <sup>d</sup>
GLC	1.88	11.73	4939	
PYR	-0.13	0.48	72	
LAC	-1.55	9.84	750	
ALA	-0.57	1.73	268	
GLR	-3.42			0.171
FA	-8.59			0.030
O <sub>2</sub>	19.82			0.615
CO <sub>2</sub>	-18.03			0.072

<sup>a</sup> $J_{b \leftrightarrow c,i}$ , net mass transport flux across the blood–cell exchange barrier ( $\mu\text{mol min}^{-1} \text{kg wet tissue}^{-1}$ ). Negative values mean the release of corresponding substrate from tissue and vice versa. Data are from *in vivo* human studies (Coppack et al., 1990; Frayn et al., 1994) except for the one for ALA (-0.57), which is from the references (Coppack et al., 1996; Patterson et al., 2002).

<sup>b</sup> $T_{max,i}$ , maximum mass transport coefficient of substrate  $i$  ( $\mu\text{mol min}^{-1} \text{kg wet tissue}^{-1}$ ).

<sup>c</sup> $M_{m,i}$ , Michaelis–Menten (M=M) constant of substrate  $i$  ( $\mu\text{M}$ ).

<sup>d</sup> $\gamma_i$ , mass transport coefficient of substrate  $i$  ( $\text{l min}^{-1} \text{kg wet tissue}^{-1}$ ).

Table 3  
Basal reaction flux rates and associated parameters for irreversible reaction fluxes

Fluxes	Flux rate <sup>a</sup>	$V_{X \rightarrow V}$ <sup>a</sup>	$K_m$ <sup>b</sup>	$K_i$ <sup>b</sup>	$\mu^{\pm c}$	$v^{\pm c}$
$\phi_{GLC \rightarrow G6P}$	1.88	4.06	460,000 <sup>e</sup>	570		
$\phi_{G6P \rightarrow GAP}$	1.88	7.53	570		0.72 (–)	
$\phi_{GAP \rightarrow PYR}$	3.56	28.44	216,000 <sup>e</sup>		0.72 (–)	9 (–)
$\phi_{PYR \rightarrow G3P}$	0.21	1.66	250		1.39 (+)	0.11 (+)
$\phi_{GLR \rightarrow G3P}$	0.01	0.02	1,012,000 <sup>e</sup>			
$\phi_{ALA \rightarrow PYR}$	2.08	4.16	1300			
$\phi_{Proteolysis}$	2.65 <sup>d</sup>	2.65				
$\phi_{PYR \rightarrow ACoA}$	3.74	22.46	50,000 <sup>e</sup>	25		9 (–)
$\phi_{FA \rightarrow FAC}$	1.70	6.82	200,000 <sup>e</sup>		1.39 (+)	
$\phi_{FAC \rightarrow ACoA}$	0.42	2.55	16,000 <sup>e</sup>	25		9 (–)
$\phi_{TG \rightarrow DG, ATGL}$	3.35	3.38	10			
$\phi_{TG \rightarrow DG, HSL}$	0.65	0.66	10			
$\phi_{DG \rightarrow MG, HSL}$	3.29	6.58	2000			
$\phi_{MG \rightarrow GLR, HSL}$	0.33	0.66	200			
$\phi_{MG \rightarrow GLR, MGL}$	2.67	29.37	2000			
$\phi_{G3P - FAC \rightarrow DG}$	0.43	0.85	104,000 <sup>e</sup>			
$\phi_{DG - FAC \rightarrow TG}$	0.43	0.85	160,000 <sup>e</sup>			
$\phi_{DG - DG \rightarrow TG}$	0.60	1.20	2000			
$\phi_{MG - MG \rightarrow DG}$	0.32	0.64	200			
$\phi_{MG - DG \rightarrow TG}$	0.27	0.54	400,000 <sup>e</sup>			
$\phi_{ACoA \rightarrow CO_2}$	7.14	57.15	67,500 <sup>e</sup>		0.72 (–)	9 (–)
$\phi_{O_2 \rightarrow H_2O}$	19.82	79.32	27 <sup>e</sup>		0.72 (–)	0.11 (+)
$\phi_{ATP \rightarrow ADP}$	125.40	376.19	4600	15,180,000 <sup>e</sup>		
$\phi_{TG \rightarrow GLR, LPL}$	0.61	0.62	10			

<sup>a</sup>Values are in  $\mu\text{mol min}^{-1} \text{kg wet tissue}^{-1}$ .  $V_{max,k}$ , maximum rate coefficient.

<sup>b</sup>Values are in  $\mu\text{mol kg wet tissue}^{-1}$  except for the marked superscript e, which are in  $(\mu\text{mol kg wet tissue}^{-1})^2$ .  $K_{m,k}$ , phenomenological M–M constant for the reactants;  $K_{i,k}$ , phenomenological M–M constant for the product inhibition.

<sup>c</sup>Values are dimensionless. (+) represent  $\mu^+$  or  $v^+$ , while (–) represent  $\mu^-$  or  $v^-$ ;  $\mu^\pm$  and  $v^\pm$  are the parameters for the metabolic controllers.

<sup>d</sup>Data are from references Coppack et al. (1996); and Patterson et al. (2002).

Table 4  
Basal reaction flux rates and associated parameters for reversible reaction fluxes

Fluxes	Flux rate <sup>a</sup>	$V_{f, X \leftrightarrow V}$ <sup>b</sup>	$V_{b, X \leftrightarrow V}$ <sup>b</sup>	$K_{f, X \leftrightarrow V}$ <sup>c</sup>	$K_{b, X \leftrightarrow V}$ <sup>c</sup>	$K_{eq, X \leftrightarrow V}$ <sup>d</sup>
$\phi_{PYR \leftrightarrow LAC}$	1.55 <sup>e</sup>	4.67	0.023	12,500	648,000	$1.06 \times 10^4$
$\phi_{GAP \leftrightarrow G3P}$	0.21	0.62	$3.3 \times 10^{-7}$	4000	585,000	$2.77 \times 10^8$

<sup>a</sup>Values are in  $\mu\text{mol min}^{-1} \text{kg wet tissue}^{-1}$ .

<sup>b</sup> $V_{f,k}$  and  $V_{b,k}$ , forward and reverse rate coefficients ( $\mu\text{mol min}^{-1} \text{kg wet tissue}^{-1}$ ).

<sup>c</sup> $K_{f,k}$  and  $K_{b,k}$ , phenomenological M–M constants for reactants and products ( $\mu\text{mol kg wet tissue}^{-1})^2$ .

<sup>d</sup> $K_{eq}$ , equilibrium constant calculated from the Gibbs free energy of reaction (dimensionless), which is from reference Alberty (2003).

<sup>e</sup>From Coppack et al. (1990).

volume are difficult to quantify. However, their levels in the intracellular water of adipocyte have been shown to be comparable to those in other tissues (Denton et al., 1966). When data of adipose tissue were not available, we used the concentrations in skeletal muscle (Table 6). The phenomenological M–M parameters,  $K_{m,k}$ ,  $K_{i,k}$ ,  $K_{f,k}$  and  $K_{b,k}$  were set to the initial tissue concentrations of the corresponding substrates. The maximum metabolic rate coefficients for irreversible reactions,  $V_{max,k}$  were calculated from basal flux, tissue concentration, and  $K_{m,k}$  (Table 3). The equilibrium constant was also utilized to calculate the forward and reverse rate coefficients ( $V_{f,k}$  and  $V_{b,k}$ ) for reversible reactions (Table 4). Mass transport coefficients ( $T_{max,i}$  and  $\gamma_i$ ) were computed from AVDs, blood flow rate,

and concentrations in arterial blood and tissue. The parameter  $\lambda_k$  must be optimally estimated using data from *in vivo* epinephrine infusion studies in humans. Other model parameters are listed in Table 7.

### 2.7. Model simulation for epinephrine infusion

Corresponding to *in vivo* studies (Samra et al., 1996), the epinephrine infusion was simulated with a constant rate infusion for 60 min (Samra et al., 1996). Since the tissue responds to the epinephrine levels in the interstitial fluid, the epinephrine levels in adipose venous outflow were used to stimulate the cellular metabolic reactions. The epinephrine levels in the adipose tissue vein and in the adipose tissue

Table 5  
Arterial and venous substrate concentrations

Substrate	Arterial concentration <sup>a,b</sup>	Venous concentration <sup>a,d</sup>
GLC	5000	4939
PYR	68	72
LAC	700	750
ALA	192	282
GLR	70	200
FA	660	719
TG	990	970
O <sub>2</sub> (total)	8000	7360
O <sub>2</sub> (free)	84 <sup>c</sup>	66 <sup>c</sup>
CO <sub>2</sub> (total)	21,700	22,218
CO <sub>2</sub> (free)	1124 <sup>c</sup>	1151 <sup>c</sup>

<sup>a</sup>Values are in  $\mu\text{M}$ .

<sup>b</sup>Data are from Kim et al. (2007).

<sup>c</sup>Free concentrations of O<sub>2</sub> and CO<sub>2</sub> are calculated from the equations given in Supplementary Material.

<sup>d</sup>Venous concentrations are calculated from the corresponding arteriovenous difference and arterial concentration data.

Table 6  
Substrate concentration in the cellular compartment

Substrate	Concentration <sup>a</sup>	References
GLC	2540	Tiessen et al. (2002)
PYR	250	Denton et al. (1966)
LAC	1440	Jansson et al. (1994)
ALA	1300 <sup>c</sup>	Kim et al. (2007)
GLR	220	Jansson et al. (1994), Stumvoll et al. (2000)
FA	1000	
TG	990,000 <sup>b</sup>	Albright and Stern (1998)
O <sub>2</sub>	34 <sup>c</sup>	Dash and Bassingthwaighe (2006), Popel (1989)
CO <sub>2</sub> (total)	15,427 <sup>c</sup>	Dash and Bassingthwaighe (2006), Geers and Gros (2000)
CO <sub>2</sub> (free)	1403 <sup>c</sup>	Dash and Bassingthwaighe (2006), Geers and Gros (2000)
G6P	570	Denton et al. (1966)
GAP	80 <sup>c</sup>	Kim et al. (2007)
G3P	1300	Denton et al. (1966)
ACoA	25	Denton and Halperin (1968)
FAC	80	Denton and Halperin (1968)
CoA	200	Denton and Halperin (1968)
DG	2000 <sup>b</sup>	Arner and Ostman (1974)
MG	200 <sup>b</sup>	Arner and Ostman (1974)
ATP	4600	Denton et al. (1966)
ADP	3300	Denton et al. (1966)
Pi	2700 <sup>c</sup>	Kim et al. (2007)
NAD <sup>+</sup>	450 <sup>c</sup>	Kim et al. (2007)
NADH	50 <sup>c</sup>	Kim et al. (2007)

<sup>a</sup>Values are in  $\mu\text{M}$  and based on the volume of intracellular water.

<sup>b</sup>Values are in  $\mu\text{M}$  and based on the total cellular volume.

<sup>c</sup>Values are from skeletal muscle studies.

were assumed to be in equilibrium. However, epinephrine infusion modulated the blood flow to adipose tissue as well as the arterial glycerol and FA concentrations, while the arterial levels of other metabolites were kept constant (Samra et al., 1996). Thus, venous epinephrine concentration ( $C_{v,Epi}$ ), adipose tissue blood flow ( $Q$ ), and arterial

Table 7  
Miscellaneous model parameters<sup>a</sup>

	Values
$K_{m,Q}$ ( $\text{ml min}^{-1} \text{kg}^{-1}$ )	31
$\alpha$ ( $\text{nM}^2$ )	0.04
$Q_0$ ( $\text{ml min}^{-1} \text{kg}^{-1}$ )	0.031 <sup>b</sup>
$C_{v,Epi,0}$ ( $\text{nM}$ )	0.1 <sup>b</sup>

<sup>a</sup> $K_{m,Q}$ , phenomenological M–M constants for LPL reaction;  $\alpha$ , parameter for epinephrine action;  $Q_0$ , adipose tissue blood flow at basal state;  $C_{v,Epi,0}$ , epinephrine concentration in adipose tissue vein at basal state.

<sup>b</sup>From the references Samra et al. (1996) and Jansson et al. (1994).

substrate concentrations for glycerol and FA ( $C_{a,GLR}$ ,  $C_{a,FA}$ ) were the only input functions for model simulation (Fig. 2). These empirical relations are shown in Table 8.

## 2.8. Simulation strategies

The effect of intracellular compartmentation of chemical species was examined by modulating the cellular volume fraction ( $v_{cf}$ ). As a comparative reference, simulations were conducted of ‘localized’ (i.e., optimally estimated  $v_{cf}$ ) and of ‘non-localized’ responses (i.e.,  $v_{cf} = 0.8$ ). Also, the effects of activation with different values of  $\lambda_k$  (i.e., differential activation) and with equal values of  $\lambda_k$  (i.e., uniform activation) were compared. The effects of different ratios of glycolysis and glyceroneogenesis on the synthesis of G3P were simulated during epinephrine infusion. An equal ratio (1:1) of these processes was assumed for the basal state.

## 2.9. Parameter estimation and numerical solution

Values of the volume fraction of cellular compartment ( $v_{cf}$ ), hormonal control ( $\lambda_k$ ) and parameters of the model input functions were estimated by minimizing the sum of squared errors between the experimental data and the corresponding simulated outputs in response to epinephrine infusion. The experimental data from studies in humans, included AVDs of glycerol, FA and TG across the inguinal fat bed *in vivo* and the concentration dynamics of glycerol and FA in the venous blood draining the inguinal fat bed (Samra et al., 1996). The model equations were numerically solved using a stiff ordinary differential equation solver, ‘ode15s’ (MATLAB<sup>®</sup>, The MathWorks Inc.). Optimal estimates of the model and input parameters were obtained using ‘lsqcurvefit’ (MATLAB<sup>®</sup>) with ‘ode15s’.

## 2.10. Sensitivity analysis

The sensitivity of the model parameters was quantified by the change in the sum of squared differences between simulated model outputs with different parameter values. Since a thorough statistical analysis of all the model

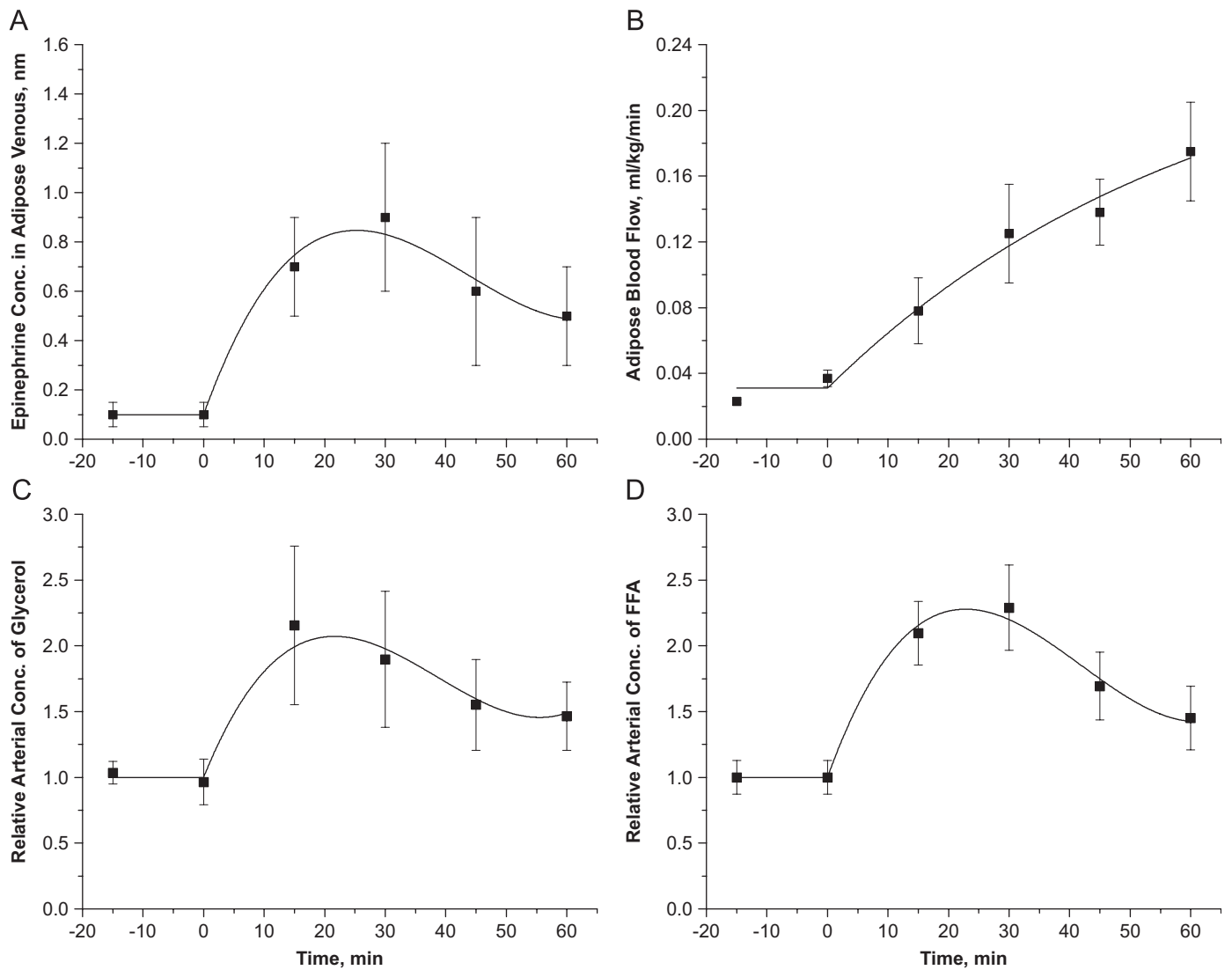


Fig. 2. Dynamic changes in (A) epinephrine concentration in adipose tissue vein, (B) adipose tissue blood flow, and (C and D) relative arterial concentrations of glycerol and FA following the intravenous infusion of epinephrine at time 0. Relative arterial concentration is the ratio of arterial concentrations at any time  $t > 0$  to  $t = 0$ . Squares represent the experimental data (mean  $\pm$  S.E.M.) of Samra et al. (1996). Solid lines are the model simulations.

Table 8  
Model input functions<sup>a</sup>

Time (min)	Input functions
$t \leq 15$	$Q = Q_0, \quad C_{v,Epi} = C_{v,Epi,0}, \quad C_{a,GLR} = C_{a,GLR,0}, \quad C_{a,FFA} = C_{a,FFA,0}$ $Q = Q_0(1 + 7.32(1 - e^{-(t-15)/62.317}))$
$t > 15$	$C_{v,Epi} = C_{v,Epi,0} + 6.837 \times 10^{-2}(t - 15) - 1.903 \times 10^{-3}(t - 15)^2 + 1.453 \times 10^{-5}(t - 15)^3$ $C_{a,GLR} = C_{a,GLR,0} + 7.979(t - 15) - 0.256(t - 15)^2 + 0.002(t - 15)^3$ $C_{a,FA} = C_{a,FA,0} + 84.486(t - 15) - 2.544(t - 15)^2 + 0.02(t - 15)^3$

<sup>a</sup>Parameters for the input functions were optimally estimated based on the data from the human *in vivo* study (Samra et al., 1996).  $Q$ , blood flow to the adipose tissue;  $C_{v,Epi}$ , epinephrine concentration in the vein;  $C_{a,GLR}$ ,  $C_{a,FA}$ , arterial glycerol and FA concentrations. Time courses of these input functions are shown in Fig. 2.

parameters is not feasible, parameter sensitivity directly related to the lipid mobilization was investigated by perturbing parameter individually. A sensitivity index for  $i$ th parameter,  $\theta_i$  can be computed as done previously (Beard, 2005):

$$S_i = \max \left( \frac{|E(\theta_i^* + 0.1\theta_i^*) - E(\theta_i^*)|}{0.1E(\theta_i^*)} \right), \quad (11)$$

where  $S_i$  is a sensitivity index;  $E$  is the sum of squared residuals for a model output;  $\theta_i^*$  is the  $i$ th parameter at its optimum. This equation represents the changes in the model output in response to 10% change in a specific parameter from its optimum.

### 3. Results

#### 3.1. Basal state analysis

The metabolic flux rates during basal state were estimated using the dynamic mass balance equations at steady state (Tables 3 and 4). Approximately 45% ( $0.8 \mu\text{mol min}^{-1} \text{kg}^{-1}$ ) of glucose taken up by adipose tissue was released as lactate and pyruvate ( $J_{PYR,b \leftrightarrow c} + J_{LAC,b \leftrightarrow c}$ , Table 2), ~5% was utilized to synthesize G3P for re-esterification of fatty acids ( $\phi_{GAP \leftrightarrow G3P}$ , Table 4), and ~50% was oxidized ( $\phi_{PYR \leftrightarrow AC0A}$ , Table 3). When the activities of HSL for TG and MG breakdown were based on that of DG breakdown, it showed that ~84% of TG breakdown was catalyzed by ATGL ( $\phi_{TG \rightarrow DG, ATGL} / (\phi_{TG \rightarrow DG, ATGL} + \phi_{TG \rightarrow DG, HSL})$ ) and ~89% of MG breakdown was catalyzed by MGL ( $\phi_{MG \rightarrow GLR, MGL} / (\phi_{MG \rightarrow GLR, HSL} + \phi_{MG \rightarrow GLR, MGL})$ ) with an insignificant contribution by HSL (Table 3). VLDL-TG breakdown by LPL in the blood compartment comprised 13% of total TG breakdown in adipose tissue bed ( $\phi_{TG \rightarrow GLR, LPL} / (\phi_{TG \rightarrow DG, ATGL} + \phi_{TG \rightarrow DG, HSL} + \phi_{TG \rightarrow GLR, LPL})$ , Table 3). The total production of FA by lipolysis in the tissue was  $10.3 \mu\text{mol min}^{-1} \text{kg}^{-1}$  ( $\phi_{TG \rightarrow DG, ATGL} + \phi_{TG \rightarrow DG, HSL} + \phi_{DG \rightarrow MG, HSL}$ , Table 3): ~84% of FA were released into the circulation ( $J_{FA, b \leftrightarrow c}$ , Table 2), ~12% was re-esterified ( $\phi_{G3P-FAC \rightarrow DG} + \phi_{DG-FAC \rightarrow TG}$ ) and ~4% was oxidized ( $\phi_{FAC \rightarrow AC0A}$ ) (Table 3). In contrast, ~99.7% of glycerol produced was released into the circulation ( $J_{FA, b \leftrightarrow c}$ , Table 2) with insignificant re-utilization within the tissue ( $\phi_{GLR \rightarrow G3P}$ , Table 3).

#### 3.2. Effect of change in lipase activity

Beginning with the basal model parameters, the basal maximum rate constants ( $V_{max}$ ) for HSL and ATGL were modulated to simulate the effect of change in lipase activity.  $V_{max}$  for HSL reactions ( $V_{max, HSL, TG \rightarrow DG}$ ,  $V_{max, HSL, DG \rightarrow MG}$ ,  $V_{max, HSL, MG \rightarrow GLR}$ ) were modulated in order to examine the effect of over- and under-expression of the enzyme. Multiplying the  $V_{max}$  with a factor smaller than one represents knockdown of the expression of the corresponding enzyme, while multiplying with a factor larger than one represents over-expression. The new

steady-state flux rates were determined after the model parameters were perturbed. Similarly, the steady-state fluxes for the reaction catalyzed by ATGL ( $V_{max, ATGL, TG \rightarrow DG}$ ) were determined.

Fig. 3A shows rates of release of FA and glycerol at the steady state in relation to the change in activities of HSL and ATGL relative to control value (= 1). A decrease in the activity of ATGL to zero lowered the rate of release of FA by 88%, while a decrease in the activity of HSL caused a 68% reduction in the release rate of FA. The rate of release of glycerol decreased by 76% associated with HSL and 66% associated with ATGL. As shown in Fig. 3B, the model simulations showed a six-fold increase in concentration of DG (relative to control) with decreasing HSL activity. In contrast, DG concentration decreased by ~85% with decreasing ATGL activity because of the lower production of DG from TG hydrolysis by ATGL.

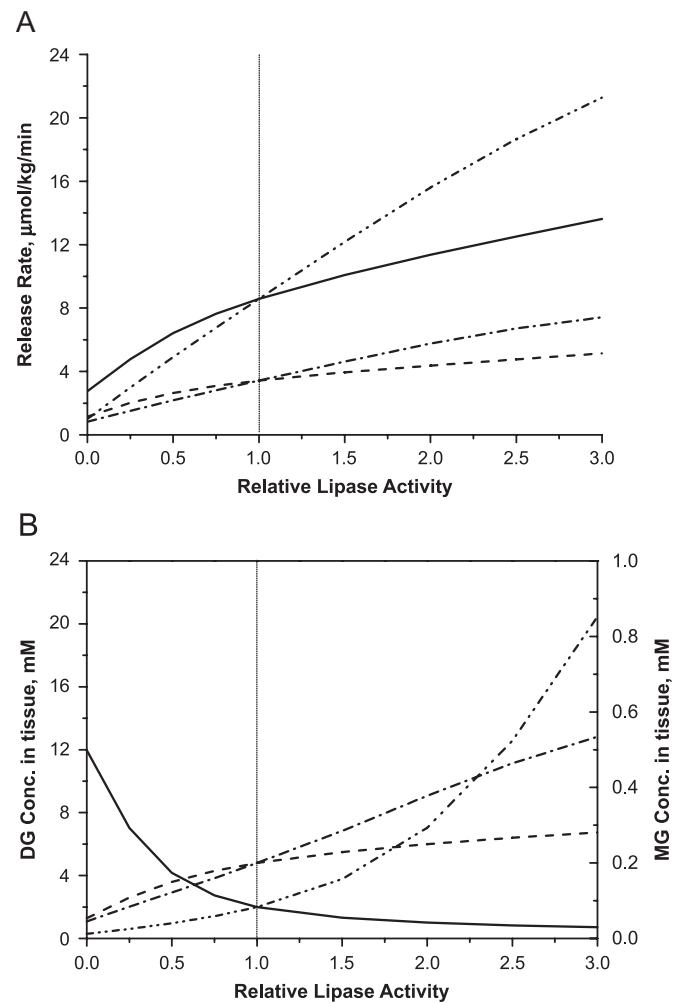


Fig. 3. Effect of varying levels of lipase expression in the basal state on (A) the rates of releases of FA (solid: HSL, dash double dotted: ATGL) and glycerol (dashed: HSL, dash dotted: ATGL) and (B) the tissue concentrations of DG (solid: HSL, dash double dotted: ATGL) and MG (dashed: HSL, dash dotted: ATGL). Relative lipase activity is the enzyme activity of ATGL or HSL relative to the control value.

There was no significant difference in the tissue concentration of MG as a result of varying enzyme activities.

Over-expressing ATGL increased the rates of release of both FA and glycerol more than those with the over-expression of HSL (~150% in ATGL vs. ~50% in HSL). The magnitude of increase was higher for FA (150% increase) than for glycerol (120% increase). The higher production of DG as a result of TG hydrolysis by ATGL resulted in the accumulation of DG. In contrast, the over-expression of HSL resulted in a higher rate of breakdown

of DG relative to TG hydrolysis and, consequently, lower tissue levels of DG. The levels of MG were increased by higher activities of both ATGL and HSL.

### 3.3. Model validation and intracellular compartmentation

Model simulations showed that epinephrine infusion increased glycerol (approximately three-fold) and FA (approximately four-fold) release rates (i.e., AVD) from adipose tissue into the circulation (Fig. 4A and B).

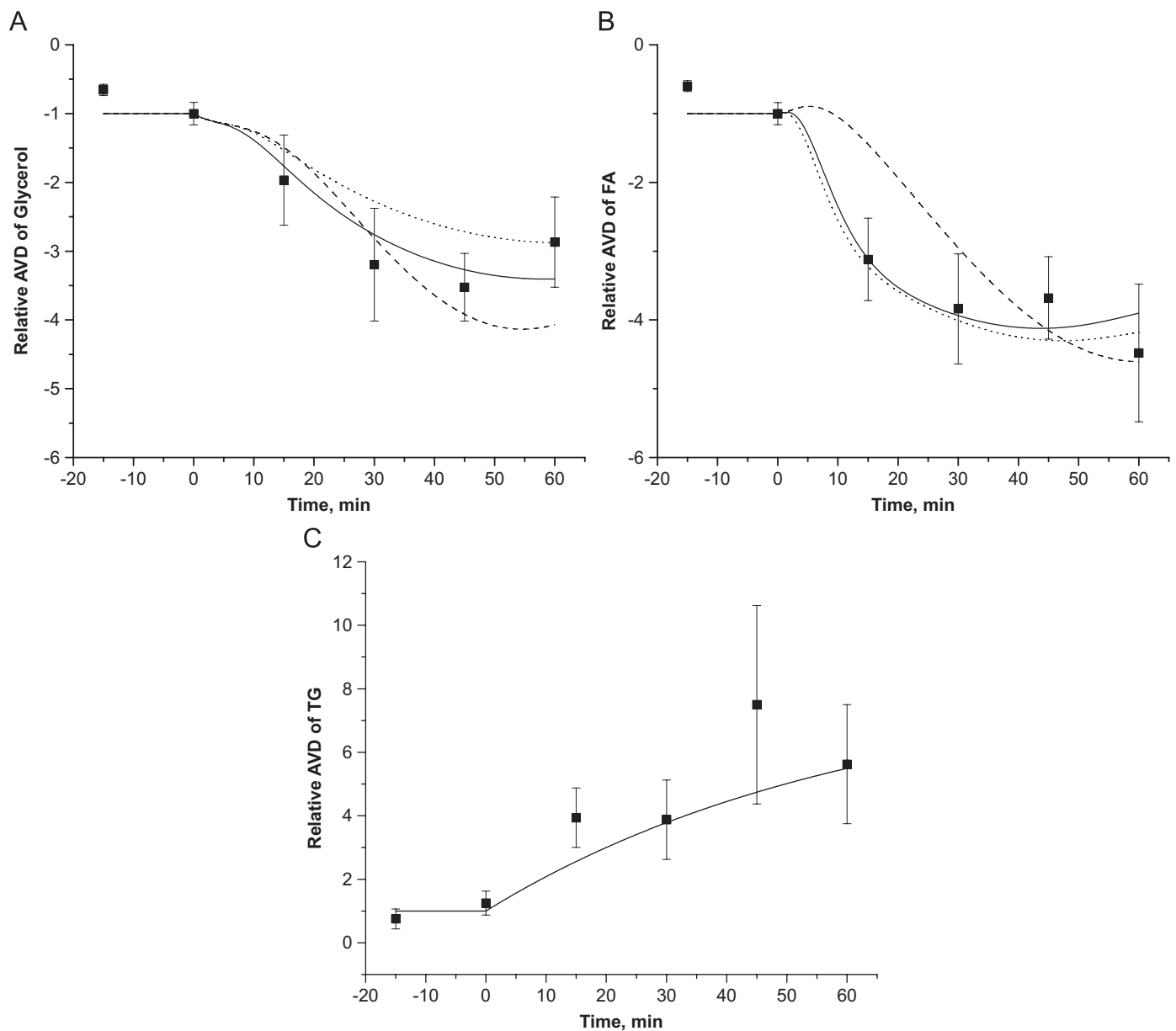


Fig. 4. (A, B) Effect of intracellular compartmentation and differential activation of lipases on dynamic exchanges of glycerol and FA across adipose tissue bed in response to the intravenous infusion of epinephrine. Relative AVD =  $AVD(t)/AVD(0)$ , is the ratio of arteriovenous differences (AVD) at any time  $t > 0$  to  $t = 0$ . Squares represent the experimental data (mean  $\pm$  S.E.M.) of Samra et al. (1996). Solid (localized, differential), dotted (localized, uniform) and dashed (unlocalized, differential) lines are the model simulations according to the localized ( $V_{cf} = 0.031$ ) or unlocalized ( $V_{cf} = 0.8$ ) metabolic subdomain and the uniform (same  $\lambda_k$ ) or differential (different  $\lambda_k$ ) activation of intracellular lipases. (C) Dynamic exchanges of TG across adipose tissue bed in response to the intravenous infusion of epinephrine. Squares represent the experimental data (mean  $\pm$  S.E.M.) of Samra et al. (1996). Solid line is the model simulation.

Table 9  
Estimated model parameters<sup>a</sup>

Parameters	Differential activation	Uniform activation
$\lambda_{TG \rightarrow DG, ATGL}$	0.72	3.18
$\lambda_{TG \rightarrow DG, HSL}$	0.91	3.18
$\lambda_{DG \rightarrow MG, HSL}$	6.19	3.18

<sup>a</sup>Values are dimensionless.

Simulated AVD responses are in agreement with the experimental data assuming localized metabolism ( $v_{cf} = 0.031$ ) and differential activation of lipases (i.e.,  $\lambda_k$ ) with parameter values in Table 9. The effect of  $v_{cf}$  on glycerol AVD was much less than that on FA AVD. When the lipase reactions were not localized ( $v_{cf} = 0.8$ ), the initial increase in FA release rate was slower and 30–50% smaller than that found experimentally (Fig. 4A and B). Model simulation showed that the breakdown of plasma TG by LPL, as indicated by AVD, gradually increased by a factor of 5 (Fig. 4C). Both glycerol and FA concentrations in the venous blood reached maximal values around ~25 min with 20% and 70% increases, but returned to basal values at the end of epinephrine infusion (Fig. 5). The localization of lipase reactions had minimal effect on the response of glycerol in the venous blood (Fig. 5A). However, the initial dynamics of FA (up to 30 min) were much slower without localization ( $v_f = 0.8$ ) resulting in 10–20% lower venous levels (Fig. 5B).

### 3.4. Regulation of lipase activities

The parameter values for which the model simulations produced the best fit to experimental data are listed in Table 9 for differential and uniform activation ( $\lambda_k$ ). In the former, the optimal estimates for  $\lambda_k$  indicate that the activation of lipolytic reactions catalyzed by HSL and ATGL increased by 1.7- to 7.2-fold. The activation required to convert DG to MG by HSL ( $\lambda_k = 6.2$ ) was approximately four times larger ( $\lambda_k = 0.7$ – $0.9$ ) than for other reactions. With uniform activation ( $\lambda_k = 3.18$ ), all lipase reactions were increased by the 4.18-fold. Figs. 3 and 4 show the effect of different lipase regulations in response to epinephrine infusion. When the metabolic reactions were localized ( $v_f = 0.031$ ), the AVD and the venous concentration dynamics of FA were in good agreement with experimental data with both activation schemes. In contrast, the AVD of glycerol during the first 30 min was 15–20% lower with uniform activation than with differential activation. This produced lower glycerol concentration in the venous outflow (Figs. 4A and 5A).

### 3.5. MG and DG dynamics

Due to the intracellular TG–FA cycle, the simulated ratio of FA to glycerol released from adipose tissue cells

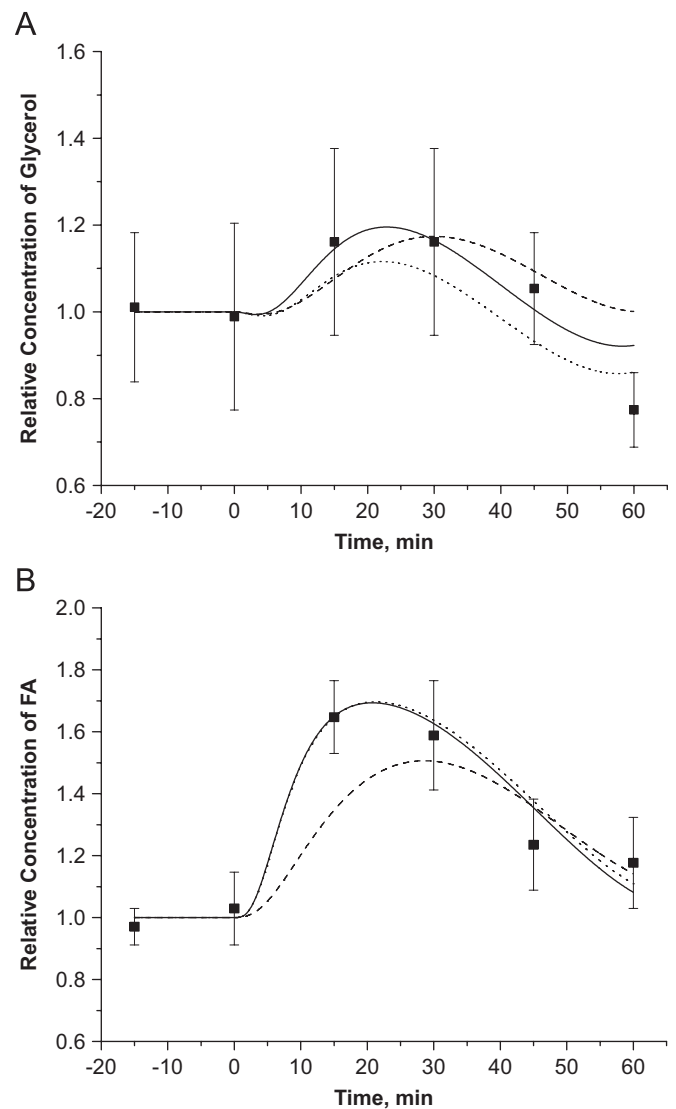


Fig. 5. Effect of intracellular compartmentation and differential activation of lipases on changes in relative concentration of glycerol (A) and FA (B) in adipose venous blood during the intravenous infusion of epinephrine. Relative concentration is the ratio of concentrations at any time  $t > 0$  to  $t = 0$ . Squares represent the experimental data (mean  $\pm$  S.E.M.) of Samra et al. (1996). Solid (localized, differential), dotted (localized, uniform) and dashed (unlocalized, differential) lines are the model simulations according to the localized ( $V_{cf} = 0.031$ ) or unlocalized ( $V_{cf} = 0.8$ ) metabolic subdomain and the uniform (same  $\lambda_k$ ) or differential (different  $\lambda_k$ ) activation of intracellular lipases.

into the blood circulation at basal state,  $J_{FA,b \leftrightarrow c} / J_{GLR,b \leftrightarrow c} \sim 2.5$  (Fig. 6A) was lower than the theoretical maximum ratio of 3. However, this ratio increased above the theoretical maximum of 5.6 at 8 min and then gradually decreased to 2.8 at 60 min. A ratio above 3 indicates an accumulation of the glycerol moiety in adipose tissue as DG and/or MG. Therefore, the model can be used to predict the major contributors to the accumulation of glycerol by simulating the tissue dynamics of lipolytic intermediates (DG and MG). Model simulations showed that MG continuously accumulated in tissue during

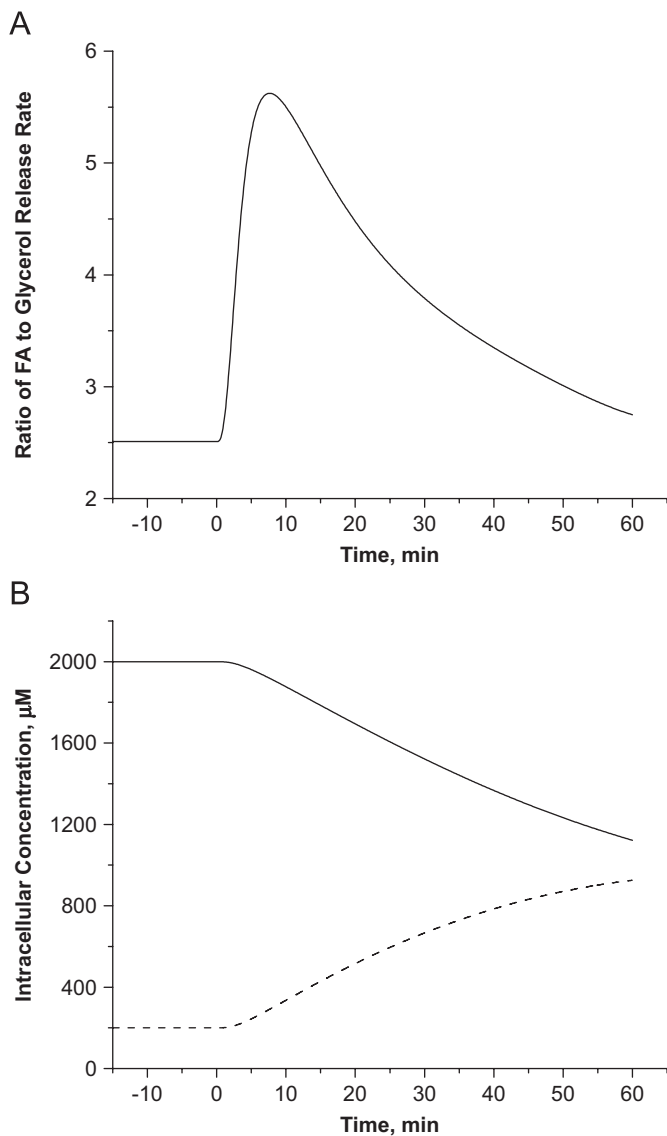


Fig. 6. Model-simulated ratio of FA to glycerol released by the adipose cellular compartment (i.e.,  $J_{FA,b \leftrightarrow c}/J_{GLR,b \leftrightarrow c}$ ) (A) and changes in intracellular lipolytic intermediates (i.e., DG, solid line; MG, dashed line) (B) in response to the intravenous infusion of epinephrine.

epinephrine infusion (0.2–0.93 mM), while DG levels decreased from 2 to 1.1 mM (Fig. 6B).

### 3.6. Re-esterification dynamics

Increased FA availability as a result of TG breakdown in the adipose tissue resulted in a higher intracellular re-esterification rate (Fig. 7A). Model simulations showed that the re-esterification rate reached its maximum (1.45  $\mu\text{mol}/\text{kg}/\text{min}$ ) at 10 min and gradually decreased toward the basal value. An increased re-esterification rate was associated with an increased rate of G3P synthesis. The relative contribution of glyceroneogenesis to G3P synthesis increased 3–14% during epinephrine infusion regardless of its fractional contribution at the basal state (Fig. 7B).

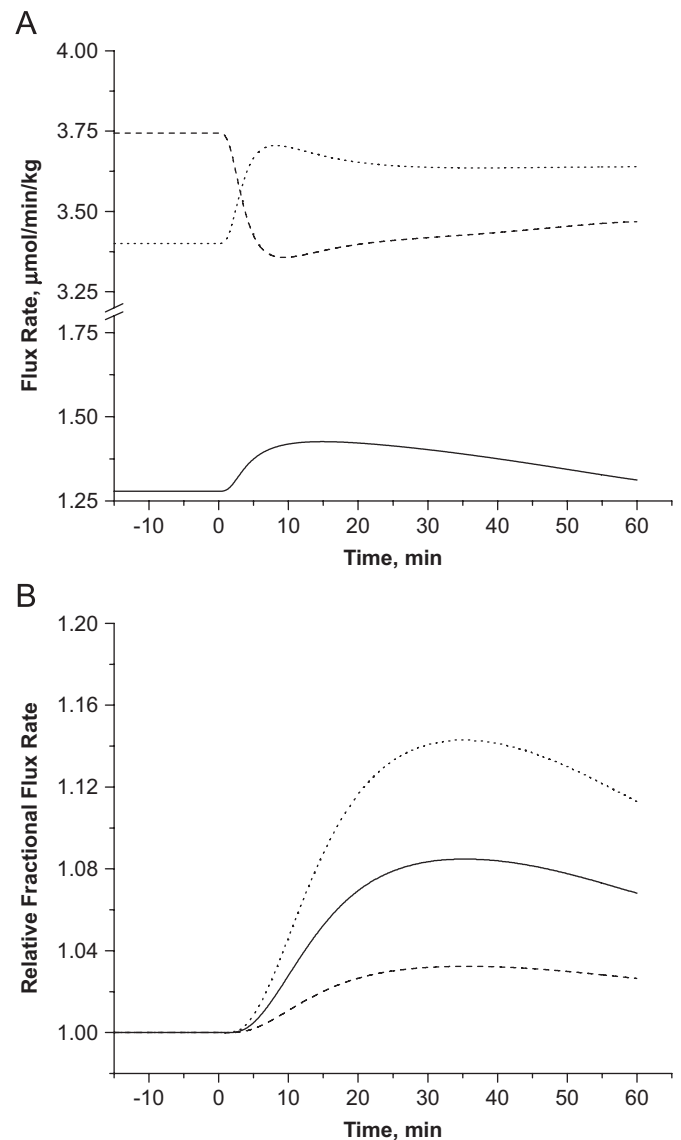


Fig. 7. (A) Model-simulated dynamic responses of FAC-dependent re-esterification rate (solid line), ACoA synthesis from pyruvate (dashed line) and FAC (dotted line). (B) Relative fractional glyceroneogenesis with different contributions at the basal state. The fractional glyceroneogenesis,  $F_{GRNG}(t) = \phi_{PYR \rightarrow G3P} / (\phi_{GAP \leftrightarrow G3P} + \phi_{PYR \rightarrow G3P})$  and the relative  $F_{GRNG}$  is the ratio of  $F_{GRNG}(t)$  at any time  $t > 0$  to  $t = 0$ . The solid line represents the equal contribution of glycolysis and glyceroneogenesis ( $F_{GRNG}(0) = 0.5$ ) while the dashed and dotted lines represent higher ( $F_{GRNG}(0) = 0.8$ ) and lower ( $F_{GRNG}(0) = 0.2$ ) contribution of glyceroneogenesis.

### 3.7. Sensitivity analysis

The sensitivity of the model parameters was quantified by the change in the sum of squared differences between simulated model outputs with different parameter values. In addition to the parameters ( $V_c$ ,  $\lambda_{ATGL,TG \rightarrow DG}$ ,  $\lambda_{HSL,TG \rightarrow DG}$ , and  $\lambda_{HSL,DG \rightarrow MG}$ ) optimally estimated from the experimental data,  $V_{max}$  and  $K_m$  for the reactions involved in lipolysis and transacylation were investigated as well. The sensitivity indices of the various model parameters are listed in Table 10. The high sensitivity indices of the parameters involved in breakdown of

Table 10  
Sensitivity indices of the model parameters related to the lipid mobilization

Parameters	Sensitivity index ( $S_i$ ) <sup>a</sup>
$v_{cf}$	0.298
$\lambda_{ATGL,TG \rightarrow DG}$	0.202
$\lambda_{HSL,TG \rightarrow DG}$	0.045
$\lambda_{HSL,DG \rightarrow MG}$	1.925
$V_{max,ATGL,TG \rightarrow DG}$	0.386
$V_{max,HSL,TG \rightarrow DG}$	0.054
$V_{max,HSL,DG \rightarrow MG}$	2.310
$V_{max,HSL,MG \rightarrow GLR}$	0.102
$V_{max,MGL,MG \rightarrow GLR}$	2.473
$K_{m,ATGL,TG \rightarrow DG}$	0
$K_{m,HSL,TG \rightarrow DG}$	0
$K_{m,HSL,DG \rightarrow MG}$	0.098
$K_{m,MGL,MG \rightarrow GLR}$	0.251
$K_{m,HSL,MG \rightarrow GLR}$	0.281
$K_{m,FAC \rightarrow G3P \rightarrow DG}$	0.282
$K_{m,DG \rightarrow TG}$	0.281
$K_{m,DG \rightarrow DG \rightarrow TG \rightarrow MG}$	0.280
$K_{m,MG \rightarrow MG \rightarrow DG \rightarrow GLR}$	0.288
$K_{m,MG \rightarrow DG \rightarrow TG \rightarrow GLR}$	0.298

<sup>a</sup>Values are dimensionless.

DG by HSL and MG by MGL (e.g.,  $\lambda_{HSL,DG \rightarrow MG}$ ,  $V_{max,HSL,DG \rightarrow MG}$  and  $V_{max,MGL,MG \rightarrow GLR}$ ) suggest that the model output is more responsive to the changes in these parameters. In contrast, the low sensitivity indices of the parameters involved in breakdown of TG by HSL and ATGL (e.g.,  $\lambda_{HSL,TG \rightarrow DG}$ ,  $V_{max,HSL,TG \rightarrow DG}$ ,  $K_{m,ATGL,TG \rightarrow DG}$  and  $K_{m,HSL,TG \rightarrow DG}$ ) suggest a minimal effect of these parameters on the model output.

#### 4. Discussion

Even though adipose tissue plays a significant role in regulating whole body fuel metabolism, it has been difficult to get reliable quantitative data (e.g., exchange of substrates) due to the heterogeneity of fat depots. Furthermore, data from various kinds of experimental studies must be integrated to get a coherent understanding of adipose tissue metabolism. Therefore, we developed a physiologically based mechanistic model of adipose tissue metabolism that includes key metabolites and regulatory enzymes in the metabolic pathways. With this model, we integrated available information on mass transport mechanisms for the tissue–blood substrate exchange, cellular metabolic pathways and their control mechanisms, as well as specific physiological characteristics of adipose tissue. Estimated parameters and dynamic responses by the model simulations were similar to those in literature and provided insight into those that cannot be estimated *in vivo*.

##### 4.1. Effect of altered expression levels of lipases

LPL catalyzes hydrolysis of VLDL-TG in the capillary bed of the adipose tissue. Until recently, HSL was

considered the only lipase responsible for hydrolyzing intracellular TG stores. However, the existence of another intracellular lipase was proposed since it was reported that HSL-deficient mice retain the basal lipolytic rate (Okazaki et al., 2002; Zechner et al., 2005; Haemmerle et al., 2002). The critical roles of this new lipase, ATGL have been shown in various studies with transgenic mice (Haemmerle et al., 2006). Due to the experimental difficulties, however, the comprehensive analysis on physiological responses in these transgenic mice could not be done, and *in vitro* studies had to be resorted for the indirect measurement. Therefore, we used the model to reproduce and predict the physiological responses arising from the genetic modulation.

As shown in Fig. 3A, the simulations confirm the important role of ATGL in regulating the basal lipolytic rate. The greater decrease of FA release by knocking down ATGL expression than that of HSL is consistent with experimental observations with transgenic mice, where ATGL-deficient mice have substantially lower levels of plasma FA (60% lower than the control) in association with massive accumulation of lipid (Haemmerle et al., 2006). In contrast, HSL-deficient mice have moderate reduction (10–20%) in the plasma FA levels without significant decrease in the basal lipolytic rate (Wang et al., 2001). As expected from the fact that DG can be hydrolyzed only by HSL, it was shown that DG accumulated in the adipose tissue of HSL-deficient mice (Haemmerle et al., 2002).

The model simulations, which were in good agreement with experimental observations, provided additional information on the lipolytic intermediate levels in other alterations. However, the reduction in the rate of release of FA with decreasing HSL activity seems to be higher in the model simulation because the basal lipolytic rate was unaltered in HSL-deficient mice. This discrepancy could be associated with a concomitant increase in ATGL expression of HSL-deficient mice to compensate for the decreased lipolytic rate due to the reduction in HSL activity. Indeed, when the expression of HSL was knocked out, the model was able to simulate a three-fold increase in ATGL activity that maintained the rate of release of FA from the adipose tissue (data not shown).

##### 4.2. Intracellular compartmentation

The localized metabolism in a subdomain volume of adipose tissue cells had significant impact on simulated responses. A smaller subdomain volume produced faster dynamic responses for the substrate exchange and adipose venous concentration of glycerol and FA (Figs. 4 and 5). Furthermore, the higher concentrations increased the blood–tissue concentration gradient to produce the required mass transport rate for sufficient metabolism. This effect was magnified by the initial acceleration in the rate of lipolysis in the tissue that increased intracellular concen-

trations of glycerol and FA. The localized metabolic subdomain is consistent with a small cytosolic volume due to large lipid droplet in adipocyte (Moore et al., 2005; Denton et al., 1966). Furthermore, the volume fraction of this metabolic subdomain estimated by the model corresponds to the volume fraction of intracellular water space (1–4% of total tissue volume) measured from *in vitro* studies of adipose fat pad (Denton et al., 1966; Crofford and Renold, 1965).

Recent *in vitro* studies of adipocyte lipid mobilization showed that major lipolytic enzymes and proteins are co-localized in a sub-cellular domain during beta-adrenergic stimulation (Granneman et al., 2007; Moore et al., 2005; Clifford et al., 2000). The localization of enzyme complexes reduces the transit time of metabolites which allows faster cellular dynamics (Welch and Easterby, 1994). To simulate cellular dynamic responses observed experimentally, cellular metabolites and enzymes should be localized to a metabolic subdomain of ~3% of total adipose tissue volume. Under this condition, model simulations can relate the intracellular mechanisms to the physiological response of the adipose tissue bed.

#### 4.3. Differential regulation of lipases

Regulation of lipase reaction during beta-adrenergic stimulation involves complex cellular mechanisms (Langin and Arner, 2006; Large et al., 2004). While HSL is highly regulated via reversible phosphorylation by PKA, the breakdown of TG by HSL requires co-activation of another protein called perilipin, which coats lipid droplets and prevent HSL and ATGL from hydrolyzing TG (Clifford et al., 2000). Consequently, the lipolysis of TG is an integrated process involving differential regulation of major lipases and other proteins. Only with differential activation for regulating lipase reactions did model simulations compare well with experimental data.

After 30 min of epinephrine infusion, glycerol AVD reached ~60% and FA AVD reached ~80% of their steady-state values. The faster dynamic response and higher FA production from adipose tissue (Fig. 4) is required to generate the sufficient concentration gradient for blood–tissue transport. The estimated parameter values (Table 9) show that DG breakdown by HSL required four times higher activation during beta-adrenergic stimulation than TG breakdown by ATGL and HSL. To simulate experimental data, the first and the second steps in lipid mobilization were stimulated to different extents. These data are consistent with the suggested role of perilipin in TG hydrolysis (Sztalryd et al., 2003; Londos et al., 1995).

The model was formulated using the biochemical data that MG breakdown by HSL and MGL are not subject to the activity change via phosphorylation with constant maximum rate coefficients (Large et al., 2004; Zechner et al., 2005). As a consequence, while MG levels in adipose tissue increased, DG levels in adipose tissue decreased over

time due to the greater increase in HSL activity for DG breakdown. The accumulation of either MG or DG can be expected from a ratio of glycerol to FA release rate higher than 3. However, model simulations predicted that accumulation of MG and not DG occurs (Fig. 6B). *In vitro* study of human adipose tissue showed 46–53% reduction in the DG levels during the increased lipolysis (Edens et al., 1990a), which is close to our model simulations (45% reduction). Measurement of dynamic changes of lipolytic intermediates (e.g., DG, MG) during epinephrine infusion *in vivo* will be required to confirm the model predictions of differential activation of lipase reactions.

#### 4.4. Source of G3P for re-esterification

Glyceroneogenesis, an abbreviated version of gluconeogenesis, involves the formation of G3P from precursors other than glucose or glycerol (Reshef et al., 2003). Since the adipose tissue lacks glycerol kinase, it cannot directly utilize glycerol for TG synthesis (Reshef et al., 2003). Therefore, G3P for the intracellular re-esterification of FA is formed from either glucose or pyruvate. We used the model to predict the relative contribution of glucose and pyruvate to G3P synthesis during the intravenous epinephrine infusion. In the absence of available *in vivo* human data, we assumed that glucose via glycolysis and pyruvate via glyceroneogenesis contribute equally in the basal state. Model simulations showed the effect of varying these contributions. Intracellular re-esterification increased by up to 13% during epinephrine infusion (Fig. 7A). In the absence of changes in other hormone levels during epinephrine infusion (Samra et al., 1996), the re-esterification rate was primarily regulated by the availability of substrates. Model simulation showed that the increased rate of G3P synthesis occurred with a greater contribution of glyceroneogenesis regardless of its relative contribution at the basal state. FAC levels increased ~80% (data not shown), which increased re-esterification during epinephrine infusion. Increase in FAC levels due to lipolysis resulted in an increased ratio of acetyl CoA to free CoA (~20%, data not shown), which inhibited the oxidation of pyruvate by decreasing the activity of pyruvate dehydrogenase (PDH). Indeed, Fig. 7A showed that ACoA synthesis from pyruvate decreased 12%, while that from FAC increased 13%. These responses suggest that the increased flux of glyceroneogenesis comes from reduction in pyruvate oxidation. Noting that the experimental epinephrine infusion rate did not alter the arterial glucose and insulin levels (Samra et al., 1996), an increase in the glucose uptake during epinephrine infusion is unlikely. Correspondingly, model simulation predicted a relatively small contribution of glycolysis. Overall, our model provided quantitative understanding of the change in *in vivo* metabolic flux rate induced by a physiological perturbation.

#### 4.5. Sensitivity analysis

There are four parameters (e.g.,  $\lambda_{HSL,TG \rightarrow DG}$ ,  $V_{max,HSL,TG \rightarrow DG}$ ,  $K_{m,ATGL,TG \rightarrow DG}$  and  $K_{m,HSL,TG \rightarrow DG}$ ) whose sensitivity indices are smaller than 0.1 indicating that these parameters were poorly estimated. Since two enzymes (ATGL and HSL) can hydrolyze TG, the one with the dominant contribution to the TG breakdown in the basal state (i.e., ATGL reaction) will have the higher sensitivity unless additional intracellular data are added to examine the differential effect of individual enzyme. Thus, the model parameters related to TG breakdown by HSL have low sensitivity indices. For these parameters to be estimated precisely, changes in activities of these enzymes must be measured.

The low sensitivity of  $K_m$  parameters, whose values were taken from the literature, may have resulted from the very high TG concentration in the adipose tissue. With a smaller  $K_m$  value than the substrate level, the reactions breaking down TG are of zero-order (i.e., independent of concentration). Therefore, the sensitivity indices for these  $K_m$  values were computed as zero. Note that there are three parameters whose sensitivity indices are greater than one. Two parameters relate to DG breakdown by HSL and one relates to MG breakdown by MGL. Therefore, reactions involving DG and MG breakdown have a more significant effect on the model simulations in response to the intravenous epinephrine infusion.

#### 4.6. Model limitations

This model was developed from the experimental data obtained from a local subcutaneous adipose tissue bed (Coppack et al., 1990; Frayn et al., 1989, 1991, 1994; Samra et al., 1996). Therefore, it may not simulate the whole-body kinetic responses as measured by isotopic tracer studies. In addition, we did not incorporate the heterogeneity of various adipose depots in the body. To investigate the role of adipose tissue in relation to metabolic disorders, a model that incorporates different types of adipose depots will be required to predict the integrated response of adipose tissue in the whole body.

The effect of beta-adrenergic stimulation on the rates of lipolytic reactions was simulated by changing the maximum rate coefficient ( $V_{max}$ ) of M–M metabolic flux equations. With these equations, activation of enzymatic reactions can also be achieved with lower  $K_m$  values that lead to increased substrate affinity. Although some  $K_m$  values were available from the literature, we had to assume others equal to the tissue levels of corresponding substrates. Because of the uncertainty of many  $K_m$  values, we did not simulate how variations of these would affect lipolytic reactions rates. An alternative strategy for future studies would be to incorporate detailed enzyme kinetics related to various lipase reactions, but this would introduce even more unknown parameters. To make such an analysis

worthwhile, many more experiments must be performed to obtain appropriate data.

Due to the lack of experimental data for adipose tissue, we had to use intracellular concentration data for GAP, NADH,  $NAD^+$ , Pi,  $O_2$  and  $CO_2$  from those in the skeletal muscle. It could introduce some miscomputations. However, this is unlikely to cause significant problem since the concentrations of these metabolites do not change significantly during experimental perturbations.

## 5. Conclusions

A physiologically based mathematical model of adipose tissue metabolism was developed to simulate dynamic responses to intravenous infusion of epinephrine. The model not only simulated the exchange of substrates across the tissue bed and the concentration dynamics in the venous blood for FA and glycerol, but also provided quantitative predictions on the metabolic regulation in the adipose tissue. A key finding in our study is the recognition of a metabolic subdomain in adipose tissue where most of enzymes and metabolic substrates were localized. By incorporating the mechanisms for regulating various lipase reactions to mobilize TG, the model showed that these lipase reactions were differentially activated during epinephrine infusion resulting in the distinctive dynamic responses of lipolytic intermediates. Critical experiments are needed to test model predictions of metabolic regulation in adipose tissue.

## Acknowledgments

This research was supported by a Grant (P50-GM-66309) from the National Institute of General Medical Sciences for developing the Center for Modeling Integrated Metabolic Systems. Ranjan Dash provided invaluable assistance in computing the effective volumes of oxygen and carbon dioxide.

## Appendix A. Supplementary materials

The online version of this article contains additional supplementary data. Please visit [doi:10.1016/j.jtbi.2007.12.005](https://doi.org/10.1016/j.jtbi.2007.12.005).

## References

- Alberty, R.A., 2003. Thermodynamics of Biochemical Reactions. Wiley, Hoboken, NJ.
- Albright, A.L., Stern, J.S., 1998. Adipose tissue. In: Fay, T.D. (Ed.), Encyclopedia of Sport Medicine and Science. Internet Society for Sport Science, Internet Society for Sport Science.
- Arner, P., Ostman, J., 1974. Mono-acid diacylglycerols in human adipose tissue. Biochim. Biophys. Acta 369, 209–221.
- Beard, D.A., 2005. A biophysical model of the mitochondrial respiratory system and oxidative phosphorylation. PLoS. Comput. Biol. 1, e36.

- Bradbury, M.W., 2006. Lipid metabolism and liver inflammation. I. Hepatic fatty acid uptake: possible role in steatosis. *Am. J. Physiol. Gastrointest. Liver Physiol.* 290, G194–G198.
- Brasaemle, D.L., Rubin, B., Harten, I.A., Gruia-Gray, J., Kimmel, A.R., Londos, C., 2000. Perilipin A increases triacylglycerol storage by decreasing the rate of triacylglycerol hydrolysis. *J. Biol. Chem.* 275, 38486–38493.
- Brito, S.C., Festuccia, W.L., Kawashita, N.H., Moura, M.F., Xavier, A.R., Garofalo, M.A., Kettelhut, I.C., Migliorini, R.H., 2006. Increased glyceroneogenesis in adipose tissue from rats adapted to a high-protein, carbohydrate-free diet: role of dietary fatty acids. *Metabolism* 55, 84–89.
- Clifford, G.M., Londos, C., Kraemer, F.B., Vernon, R.G., Yeaman, S.J., 2000. Translocation of hormone-sensitive lipase and perilipin upon lipolytic stimulation of rat adipocytes. *J. Biol. Chem.* 275, 5011–5015.
- Coppack, S.W., Frayn, K.N., Humphreys, S.M., Whyte, P.L., Hockaday, T.D., 1990. Arteriovenous differences across human adipose and forearm tissues after overnight fast. *Metabolism* 39, 384–390.
- Coppack, S.W., Persson, M., Miles, J.M., 1996. Phenylalanine kinetics in human adipose tissue. *J. Clin. Invest.* 98, 692–697.
- Crofford, O.B., Renold, A.E., 1965. Glucose uptake by incubated rat epididymal adipose tissue. Rate-limiting steps and site of insulin action. *J. Biol. Chem.* 240, 14–21.
- Dash, R.K., Bassingthwaite, J.B., 2006. Simultaneous blood-tissue exchange of oxygen, carbon dioxide, bicarbonate, and hydrogen ion. *Ann. Biomed. Eng.* 34, 1129–1148.
- Denton, R.M., Halperin, M.L., 1968. The control of fatty acid and triglyceride synthesis in rat epididymal adipose tissue. Roles of coenzyme A derivatives, citrate and L-glycerol 3-phosphate. *Biochem. J.* 110, 27–38.
- Denton, R.M., Yorke, R.E., Randle, P.J., 1966. Measurement of concentrations of metabolites in adipose tissue and effects of insulin, alloxan-diabetes and adrenaline. *Biochem. J.* 100, 407–419.
- Edens, N.K., Leibel, R.L., Hirsch, J., 1990a. Lipolytic effects on diacylglycerol accumulation in human adipose tissue in vitro. *J. Lipid Res.* 31, 1351–1359.
- Edens, N.K., Leibel, R.L., Hirsch, J., 1990b. Mechanism of free fatty acid re-esterification in human adipocytes in vitro. *J. Lipid Res.* 31, 1423–1431.
- Frayn, K.N., 2001. Adipose tissue and the insulin resistance syndrome. *Proc. Nutr. Soc.* 60, 375–380.
- Frayn, K.N., 2002. Adipose tissue as a buffer for daily lipid flux. *Diabetologia* 45, 1201–1210.
- Frayn, K.N., Coppack, S.W., Humphreys, S.M., Whyte, P.L., 1989. Metabolic characteristics of human adipose tissue in vivo. *Clin. Sci. (Lond.)* 76, 509–516.
- Frayn, K.N., Khan, K., Coppack, S.W., Elia, M., 1991. Amino acid metabolism in human subcutaneous adipose tissue in vivo. *Clin. Sci. (Lond.)* 80, 471–474.
- Frayn, K.N., Shadid, S., Hamlani, R., Humphreys, S.M., Clark, M.L., Fielding, B.A., Boland, O., Coppack, S.W., 1994. Regulation of fatty acid movement in human adipose tissue in the postabsorptive-to-postprandial transition. *Am. J. Physiol.* 266, E308–E317.
- Frayn, K.N., Humphreys, S.M., Coppack, S.W., 1995. Fuel selection in white adipose tissue. *Proc. Nutr. Soc.* 54, 177–189.
- Frayn, K.N., Karpe, F., Fielding, B.A., Macdonald, I.A., Coppack, S.W., 2003. Integrative physiology of human adipose tissue. *Int. J. Obes. Relat. Metab. Disord.* 27, 875–888.
- Geers, C., Gros, G., 2000. Carbon dioxide transport and carbonic anhydrase in blood and muscle. *Physiol. Rev.* 80, 681–715.
- Granneman, J.G., Moore, H.P., Granneman, R.L., Greenberg, A.S., Obin, M.S., Zhu, Z., 2007. Analysis of lipolytic protein trafficking and interactions in adipocytes. *J. Biol. Chem.* 282, 5726–5735.
- Haemmerle, G., Zimmermann, R., Hayn, M., Theussl, C., Waeg, G., Wagner, E., Sattler, W., Magin, T.M., Wagner, E.F., Zechner, R., 2002. Hormone-sensitive lipase deficiency in mice causes diglyceride accumulation in adipose tissue, muscle, and testis. *J. Biol. Chem.* 277, 4806–4815.
- Haemmerle, G., Lass, A., Zimmermann, R., Gorkiewicz, G., Meyer, C., Rozman, J., Heldmaier, G., Maier, R., Theussl, C., Eder, S., Kratky, D., Wagner, E.F., Klingenspor, M., Hoefler, G., Zechner, R., 2006. Defective lipolysis and altered energy metabolism in mice lacking adipose triglyceride lipase. *Science* 312, 734–737.
- Honnor, R.C., Dhillon, G.S., Londos, C., 1985. cAMP-dependent protein kinase and lipolysis in rat adipocytes. II. Definition of steady-state relationship with lipolytic and antilipolytic modulators. *J. Biol. Chem.* 260, 15130–15138.
- Jansson, P.A., Larsson, A., Smith, U., Lonroth, P., 1994. Lactate release from the subcutaneous tissue in lean and obese men. *J. Clin. Invest.* 93, 240–246.
- Jensen, M.D., 2002. Adipose tissue and fatty acid metabolism in humans. *J. R. Soc. Med.* 95 (Suppl. 42), 3–7.
- Jurczak, M.J., Danos, A.M., Rehrmann, V.R., Allison, M.B., Greenberg, C.C., Brady, M.J., 2007. Transgenic overexpression of protein targeting to glycogen markedly increases adipocytic glycogen storage in mice. *Am. J. Physiol. Endocrinol. Metab.* 292, E952–E963.
- Kahn, S.E., Hull, R.L., Utzschneider, K.M., 2006. Mechanisms linking obesity to insulin resistance and type 2 diabetes. *Nature* 444, 840–846.
- Karpe, F., Olivecrona, T., Olivecrona, G., Samra, J.S., Summers, L.K., Humphreys, S.M., Frayn, K.N., 1998. Lipoprotein lipase transport in plasma: role of muscle and adipose tissues in regulation of plasma lipoprotein lipase concentrations. *J. Lipid Res.* 39, 2387–2393.
- Kim, J., Saidel, G.M., Cabrera, M.E., 2007. Multi-scale computational model of fuel homeostasis during exercise: effect of hormonal control. *Ann. Biomed. Eng.* 35, 69–90.
- Klein, S., Wolfe, R.R., 1990. Whole-body lipolysis and triglyceride-fatty acid cycling in cachectic patients with esophageal cancer. *J. Clin. Invest.* 86, 1403–1408.
- Langin, D., Arner, P., 2006. Importance of TNF $\alpha$  and neutral lipases in human adipose tissue lipolysis. *Trends Endocrinol. Metab.* 17, 314–320.
- Large, V., Arner, P., Reynisdottir, S., Grober, J., Van Harmelen, V., Holm, C., Langin, D., 1998. Hormone-sensitive lipase expression and activity in relation to lipolysis in human fat cells. *J. Lipid Res.* 39, 1688–1695.
- Large, V., Peroni, O., Letexier, D., Ray, H., Beylot, M., 2004. Metabolism of lipids in human white adipocyte. *Diabetes Metab.* 30, 294–309.
- Londos, C., Brasaemle, D.L., Gruia-Gray, J., Servetnick, D.A., Schultz, C.J., Levin, D.M., Kimmel, A.R., 1995. Perilipin: unique proteins associated with intracellular neutral lipid droplets in adipocytes and steroidogenic cells. *Biochem. Soc. Trans.* 23, 611–615.
- Moore, H.P., Silver, R.B., Mottillo, E.P., Bernlohr, D.A., Granneman, J.G., 2005. Perilipin targets a novel pool of lipid droplets for lipolytic attack by hormone-sensitive lipase. *J. Biol. Chem.* 280, 43109–43120.
- Newsholme, E.A., Crabtree, B., 1976. Substrate cycles in metabolic regulation and in heat generation. *Biochem. Soc. Symp.*, 61–109.
- Okazaki, H., Osuga, J., Tamura, Y., Yahagi, N., Tomita, S., Shionoiri, F., Iizuka, Y., Ohashi, K., Harada, K., Kimura, S., Gotoda, T., Shimano, H., Yamada, N., Ishibashi, S., 2002. Lipolysis in the absence of hormone-sensitive lipase: evidence for a common mechanism regulating distinct lipases. *Diabetes* 51, 3368–3375.
- Patterson, B.W., Horowitz, J.F., Wu, G., Watford, M., Coppack, S.W., Klein, S., 2002. Regional muscle and adipose tissue amino acid metabolism in lean and obese women. *Am. J. Physiol. Endocrinol. Metab.* 282, E931–E936.
- Popel, A.S., 1989. Theory of oxygen transport to tissue. *Crit. Rev. Biomed. Eng.* 17, 257–321.
- Reshef, L., Olswang, Y., Cassuto, H., Blum, B., Croniger, C.M., Kalhan, S.C., Tilghman, S.M., Hanson, R.W., 2003. Glyceroneogenesis and the triglyceride/fatty acid cycle. *J. Biol. Chem.* 278, 30413–30416.
- Samra, J.S., Simpson, E.J., Clark, M.L., Forster, C.D., Humphreys, S.M., Macdonald, I.A., Frayn, K.N., 1996. Effects of epinephrine infusion on adipose tissue: interactions between blood flow and lipid metabolism. *Am. J. Physiol.* 271, E834–E839.
- Schweiger, M., Schreiber, R., Haemmerle, G., Lass, A., Fledelius, C., Jacobsen, P., Tornqvist, H., Zechner, R., Zimmermann, R., 2006.

- Adipose triglyceride lipase and hormone-sensitive lipase are the major enzymes in adipose tissue triacylglycerol catabolism. *J. Biol. Chem.* 281, 40236–40241.
- Shen, W.J., Patel, S., Natu, V., Kraemer, F.B., 1998. Mutational analysis of structural features of rat hormone-sensitive lipase. *Biochemistry* 37, 8973–8979.
- Stumvoll, M., Jacob, S., Wahl, H.G., Hauer, B., Loblein, K., Grauer, P., Becker, R., Nielsen, M., Renn, W., Haring, H., 2000. Suppression of systemic, intramuscular, and subcutaneous adipose tissue lipolysis by insulin in humans. *J. Clin. Endocrinol. Metab.* 85, 3740–3745.
- Sztalryd, C., Xu, G., Dorward, H., Tansey, J.T., Contreras, J.A., Kimmel, A.R., Londos, C., 2003. Perilipin A is essential for the translocation of hormone-sensitive lipase during lipolytic activation. *J. Cell Biol.* 161, 1093–1103.
- Tiessen, R.G., Rhemrev-Boom, M.M., Korf, J., 2002. Glucose gradient differences in subcutaneous tissue of healthy volunteers assessed with ultraslow microdialysis and a nanolitre glucose sensor. *Life Sci.* 70, 2457–2466.
- Tordjman, J., Chauvet, G., Quette, J., Beale, E.G., Forest, C., Antoine, B., 2003. Thiazolidinediones block fatty acid release by inducing glyceroneogenesis in fat cells. *J. Biol. Chem.* 278, 18785–18790.
- Trayhurn, P., Beattie, J.H., 2001. Physiological role of adipose tissue: white adipose tissue as an endocrine and secretory organ. *Proc. Nutr. Soc.* 60, 329–339.
- Wang, S.P., Laurin, N., Himms-Hagen, J., Rudnicki, M.A., Levy, E., Robert, M.F., Pan, L., Oligny, L., Mitchell, G.A., 2001. The adipose tissue phenotype of hormone-sensitive lipase deficiency in mice. *Obes. Res.* 9, 119–128.
- Welch, G.R., Easterby, J.S., 1994. Metabolic channeling versus free diffusion: transition-time analysis. *Trends Biochem. Sci.* 19, 193–197.
- Zechner, R., Strauss, J.G., Haemmerle, G., Lass, A., Zimmermann, R., 2005. Lipolysis: pathway under construction. *Curr. Opin. Lipidol.* 16, 333–340.
- Zhou, L., Salem, J.E., Saidel, G.M., Stanley, W.C., Cabrera, M.E., 2005. Mechanistic model of cardiac energy metabolism predicts localization of glycolysis to cytosolic subdomain during ischemia. *Am. J. Physiol. Heart Circ. Physiol.* 288, H2400–H2411.
- Zimmermann, R., Strauss, J.G., Haemmerle, G., Schoiswohl, G., Birner-Gruenberger, R., Riederer, M., Lass, A., Neuberger, G., Eisenhaber, F., Hermetter, A., Zechner, R., 2004. Fat mobilization in adipose tissue is promoted by adipose triglyceride lipase. *Science* 306, 1383–1386.